

# Bespoke library docking for 5-HT<sub>2A</sub> receptor agonists with antidepressant activity

<https://doi.org/10.1038/s41586-022-05258-z>

Received: 19 August 2021

Accepted: 22 August 2022

Published online: 28 September 2022

 Check for updates

Anat Levit Kaplan<sup>1,15</sup>, Danielle N. Confair<sup>2,15</sup>, Kuglae Kim<sup>3,4,15</sup>, Ximena Barros-Álvarez<sup>5,15</sup>, Ramona M. Rodriguiz<sup>6,7</sup>, Ying Yang<sup>1</sup>, Oh Sang Kweon<sup>2</sup>, Tao Che<sup>8</sup>, John D. McCorvy<sup>9</sup>, David N. Kamber<sup>2</sup>, James P. Phelan<sup>2</sup>, Luan Carvalho Martins<sup>1,10</sup>, Vladimir M. Pogorelov<sup>6</sup>, Jeffrey F. DiBerto<sup>3</sup>, Samuel T. Slocum<sup>3</sup>, Xi-Ping Huang<sup>11</sup>, Jain Manish Kumar<sup>3</sup>, Michael J. Robertson<sup>5</sup>, Ouliana Panova<sup>5</sup>, Alpay B. Seven<sup>5</sup>, Autumn Q. Wetsel<sup>6</sup>, William C. Wetsel<sup>6,7,12,13</sup>, John J. Irwin<sup>1</sup>, Georgios Skiniotis<sup>5</sup>, Brian K. Shoichet<sup>1</sup>, Bryan L. Roth<sup>3,14</sup> & Jonathan A. Ellman<sup>2</sup>

There is considerable interest in screening ultralarge chemical libraries for ligand discovery, both empirically and computationally<sup>1–4</sup>. Efforts have focused on readily synthesizable molecules, inevitably leaving many chemotypes unexplored. Here we investigate structure-based docking of a bespoke virtual library of tetrahydropyridines—a scaffold that is poorly sampled by a general billion-molecule virtual library but is well suited to many aminergic G-protein-coupled receptors. Using three inputs, each with diverse available derivatives, a one pot C–H alkenylation, electrocyclization and reduction provides the tetrahydropyridine core with up to six sites of derivatization<sup>5–7</sup>. Docking a virtual library of 75 million tetrahydropyridines against a model of the serotonin 5-HT<sub>2A</sub> receptor (5-HT<sub>2A</sub>R) led to the synthesis and testing of 17 initial molecules. Four of these molecules had low-micromolar activities against either the 5-HT<sub>2A</sub> or the 5-HT<sub>2B</sub> receptors. Structure-based optimization led to the 5-HT<sub>2A</sub>R agonists (*R*)-69 and (*R*)-70, with half-maximal effective concentration values of 41 nM and 110 nM, respectively, and unusual signalling kinetics that differ from psychedelic 5-HT<sub>2A</sub>R agonists. Cryo-electron microscopy structural analysis confirmed the predicted binding mode to 5-HT<sub>2A</sub>R. The favourable physical properties of these new agonists conferred high brain permeability, enabling mouse behavioural assays. Notably, neither had psychedelic activity, in contrast to classic 5-HT<sub>2A</sub>R agonists, whereas both had potent antidepressant activity in mouse models and had the same efficacy as antidepressants such as fluoxetine at as low as 1/40th of the dose. Prospects for using bespoke virtual libraries to sample pharmacologically relevant chemical space will be considered.

The advent of DNA-encoded and virtual libraries has led to a renaissance in ultralarge sets of molecules in early ligand discovery<sup>1</sup>. In particular, the virtual libraries now exceed 20 billion enumerated, readily accessible molecules. In docking screens, these virtual libraries have examined new chemotypes that are well suited to receptor sites, discovering ligands with potencies in the mid-picomolar to low-nanomolar range<sup>2–4</sup>. This represents a substantial improvement from screens of smaller, ‘in stock’ libraries of several million molecules against the same targets. The virtual libraries enumerate diverse chemotypes,

reflecting the synthetic products of more than 120,000 building-blocks synthesized through more than 140 two-component reactions. Nevertheless, the vastness of chemical space ensures that many interesting chemotypes are inevitably absent or undersampled by both virtual and DNA-encoded libraries.

The six-membered nitrogen heterocycles piperidine and pyridine are two of the top three most frequent ring systems among US Food and Drug Administration (FDA)-approved drugs (Extended Data Table 1). In particular, the non-aromatic piperidine scaffold has several desirable

<sup>1</sup>Department of Pharmaceutical Chemistry, University of California, San Francisco, CA, USA. <sup>2</sup>Department of Chemistry, Yale University, New Haven, CT, USA. <sup>3</sup>Department of Pharmacology, University of North Carolina, Chapel Hill School of Medicine, Chapel Hill, NC, USA. <sup>4</sup>Department of Pharmacy, Yonsei University, Incheon, Republic of Korea. <sup>5</sup>Department of Molecular and Cellular Physiology, Stanford University School of Medicine, Stanford, CA, USA. <sup>6</sup>Department of Psychiatry and Behavioral Sciences, Duke University Medical Center, Durham, NC, USA. <sup>7</sup>Mouse Behavioral and Neuroendocrine Analysis Core Facility, Duke University Medical Center, Durham, NC, USA. <sup>8</sup>Center for Clinical Pharmacology, Department of Anesthesiology, Washington University School of Medicine, St Louis, MO, USA. <sup>9</sup>Department of Cell Biology, Neurobiology and Anatomy, Medical College of Wisconsin, Milwaukee, WI, USA. <sup>10</sup>Biochemistry Department, Institute for Biological Sciences, Federal University of Minas Gerais, Belo Horizonte, Brazil. <sup>11</sup>National Institute of Mental Health Psychoactive Drug Screening Program, University of North Carolina Chapel Hill School of Medicine, Chapel Hill, NC, USA. <sup>12</sup>Department of Cell Biology, Duke University Medical Center, Durham, NC, USA. <sup>13</sup>Department of Neurobiology, Duke University Medical Center, Durham, NC, USA. <sup>14</sup>Division of Chemical Biology and Medicinal Chemistry, Eshelman School of Pharmacy, University of North Carolina Chapel Hill, Chapel Hill, NC, USA. <sup>15</sup>These authors contributed equally: Anat Levit Kaplan, Danielle N. Confair, Kuglae Kim, Ximena Barros-Álvarez. ✉e-mail: [william.wetsel@duke.edu](mailto:william.wetsel@duke.edu); [jjj@cgl.ucsf.edu](mailto:jjj@cgl.ucsf.edu); [yorgo@stanford.edu](mailto:yorgo@stanford.edu); [bshoichet@gmail.com](mailto:bshoichet@gmail.com); [bryan\\_roth@med.unc.edu](mailto:bryan_roth@med.unc.edu); [jonathan.ellman@yale.edu](mailto:jonathan.ellman@yale.edu)

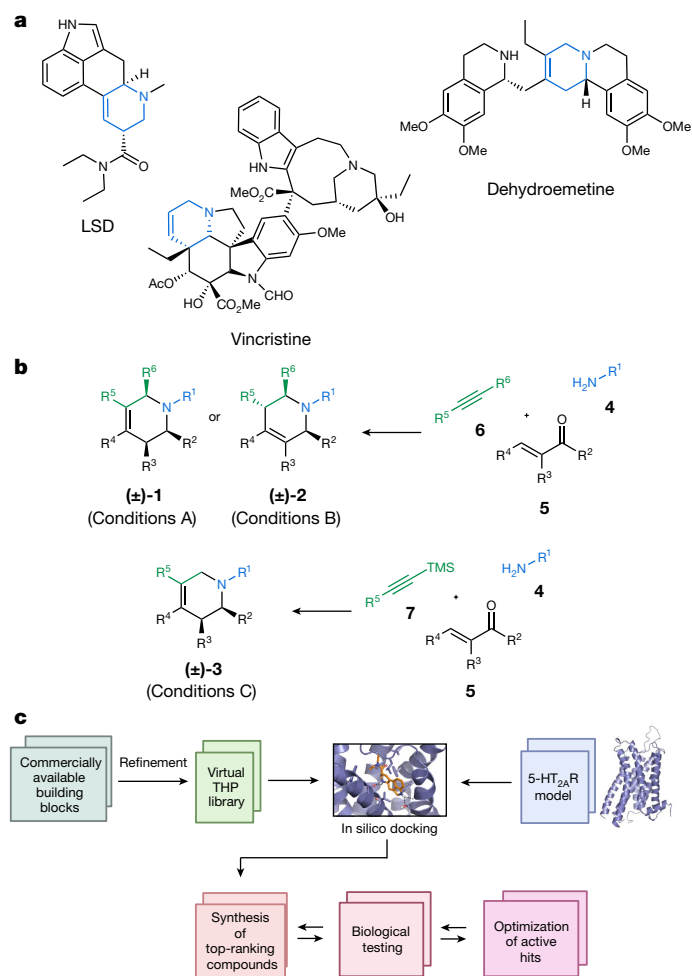


**Fig. 1 | Bespoke ultralarge virtual library approach.** **a**, Drugs containing a THP motif. **b**, Three types of THP ( $\pm$ -1 to  $\pm$ -3) from commercially available alkyne **6** and **7**, primary amines **4** and  $\alpha,\beta$ -unsaturated carbonyl compounds **5**. **c**, Generation of a virtual library of 75 million THPs for docking against a homology model of 5-HT<sub>2A</sub>R.

features, such as a basic nitrogen that contributes to aqueous solubility and hydrogen-bonding interactions, high  $sp^3$  bond content with a three-dimensional rather than planar display<sup>8</sup> and multiple sites for introducing substituents, including at stereogenic centres. Tetrahydropyridines (THPs) are a much less investigated class of six-membered nitrogen heterocycles that are intermediate in unsaturation between pyridines and piperidines with the same favourable attributes as piperidines. Although THPs are present in several natural-product-derived drugs that include the psychedelic lysergic acid diethylamide (LSD), the antimigraine drug ergotamine, anticancer agents such as vinblastine and vincristine, and the antiprotozoal agent dehydroemetine (Fig. 1a; the structure, bioactivity, literature and clinical trials of LSD, ergotamine, vinblastine, vincristine and dehydroemetine can be obtained by searching for the compound name in PubChem), the scaffold is under-represented in most libraries compared with its congeners piperidine and pyridine (Extended Data Table 1). In particular, although piperidine and pyridine occur in a notable 16–18% of the molecules in the unbiased REAL make-on-demand library, THPs comprised only 0.35% (Extended Data Table 1).

Obtaining a diverse display of functionality at different sites about the six-membered ring in piperidines and THPs is synthetically challenging. We recently described new convergent routes to access three THP subtypes ( $\pm$ -1 to  $\pm$ -3) with six sites of derivatization from commercially available starting materials<sup>5–7</sup> (Fig. 1b). The large space defined by such derivatives, their functionally congested, geometrically complex structures and their

under-representation in general libraries<sup>9</sup> (Extended Data Table 1) makes them interesting to explore as central scaffolds for large virtual libraries that are well suited to structure-based molecular docking.

Accordingly, we calculated a library of over 75 million virtual THPs, built around commercially available building blocks and restricted to products with lead-like physical properties (for example,  $\leq 350$  amu,  $c\text{LogP} \leq 3.5$ )<sup>10,11</sup>. The cationic nature of these molecules at physiological pH makes them suitable as ligands for aminergic GPCRs, including 5-HT<sub>2A</sub>R. The 5-HT<sub>2A</sub>R is a target of much interest owing to its role in treating psychiatric disorders such as schizophrenia, depression and anxiety<sup>12–14</sup>. The 5-HT<sub>2A</sub>R also represents the canonical molecular target for LSD-like psychedelic drugs<sup>15</sup>, which have recently gained prominence as potential therapeutics for depression and anxiety<sup>16</sup>. With hallucination remaining a liability, a goal in this area is the development of drug leads that retain the antidepressant and anxiolytic properties without psychedelic activity. Progress towards such leads and chemical probes against the 5-HT<sub>2A</sub>R has been slowed by the need for selectivity over related off-targets, such as 5-HT<sub>2B</sub>R, versus other receptors such as the serotonin transporter (SERT), and for functional selectivity in signalling (that is, for recruitment of G protein versus  $\beta$ -arrestin<sup>15,17–20</sup>). Collectively, these features make 5-HT<sub>2A</sub>R a therapeutically worthy yet challenging target. Meanwhile, the small and well-formed orthosteric site of the receptor<sup>15</sup> makes it a favourable target for docking this particular virtual library.

We therefore explored docking to prioritize selective 5-HT<sub>2A</sub>R ligands from among the 75 million molecule virtual library. Here we consider the mechanics of calculating a large library around a specific scaffold and reaction and synthesizing docking-prioritized molecules from such a large space, as well as whether this approach to discover and optimize potent and selective ligands is useful. The implications for the creation and exploration of bespoke libraries around interesting scaffolds more generally was also considered.

## Virtual library calculation

THP subtypes ( $\pm$ -1 and  $\pm$ -2) were prepared from three readily available inputs: primary amines **4**,  $\alpha,\beta$ -unsaturated carbonyl compounds **5** and internal alkynes **6** (Fig. 1b). THP subtype ( $\pm$ -3) was prepared from primary amines **4**,  $\alpha,\beta$ -unsaturated carbonyl compounds **5** and trimethylsilyl (TMS) alkynes **7**. A broad range of functional groups, including many different types of nitrogen heterocycle, were found to be compatible with the reaction sequence as determined by a functional group screen (Supplementary Fig. 1). Heterocycle N–H functionality was incompatible with the chemistry, but this could be overcome by straightforward *N*-protection. As a consequence, these inputs and restraints were also included in the virtual library. To simplify library synthesis and analysis, only achiral, single-isomer inputs were included. Inputs with an undesirable functionality, such as nitro groups, or molecules with too many rotatable bonds were discarded. To generate library members with drug-like physical properties, a molecular mass cut-off of 150–160 amu was applied to each of the reactants (TMS alkynes **7** were assigned a cut-off of 212 amu because the TMS group is cleaved during the synthesis). A molecular mass cut-off of 400 amu and a  $c\text{LogP}$  of  $\leq 3.5$  were then applied to the assembled THPs ( $\pm$ -1 to  $\pm$ -3) to furnish a virtual library of 4.3 billion compounds; this library would subsequently be available for selection of analogues. To maximize the likelihood of identifying hits with high ligand efficiency for the initial docking screen, we further restricted the molecular mass to  $\leq 350$  amu, resulting in an initial virtual library of 75 million molecules.

## Docking and modelling

Seeking new ligands for 5-HT<sub>2A</sub>R, we used an iterative computational and empirical screening strategy (Fig. 1c). We initially did not differentiate between agonists or antagonists, as selective compounds of either

class would be useful. As there were no X-ray or cryo electron microscopy (cryo-EM) structures of the 5-HT<sub>2A</sub>R available at the time this study was conducted, we first built 1,000 homology models templated on the 5-HT<sub>2B</sub>R X-ray structure bound to LSD, using Modeller (Protein Data Bank (PDB): 5TVN; as described in ref.<sup>20</sup>). The orthosteric ligand LSD was retained during the modelling to ensure a ligand-competent orthosteric binding site. The resulting homology models were evaluated for their ability to enrich 34 known 5-HT<sub>2A</sub>R ligands from the IUPHAR database<sup>21</sup> versus 1,899 property-matched decoys<sup>22</sup>. The models were ranked by their ability to enrich the ligands versus the decoys, in sensible geometries, among the top scoring docked molecules<sup>23,24</sup>. The models were also assessed for their ability to reproduce the crystallographic pose of LSD and to form key interactions with the receptor such as the observed salt bridge with Asp<sup>3.32</sup> (superscripts refer to the Ballesteros–Weinstein numbering system for GPCR residues, in which the first number denotes the helix and the second number indicates the residue position relative to the most conserved residue, defined as X.50<sup>25</sup>).

The best-performing 5-HT<sub>2A</sub>R model was screened against the 75 million THP library. Each library molecule had an average of 92 conformations calculated for it and was sampled in approximately 23,000 orientations. A total of 7.46 trillion complexes were sampled and scored; the calculation took 8,698 core hours, or just under 9 h on 1,000 cores of our laboratory cluster. The 300,000 top-ranking docked molecules were clustered by topological similarity using an ECFP4-based Tanimoto coefficient (Tc) > 0.5; this found 14,959 non-redundant clusters. The top-scoring molecules for the top-ranked 4,000 clusters were inspected for unfavourable features, which are sometimes not accounted for by the docking scoring function, including internal ligand strain and the occurrence of unsatisfied ligand hydrogen-bond donors, and for modelled interactions with key binding-site residues<sup>26</sup>. Of those that remained, 205 were filtered for chemical novelty by insisting on ECFP4-based Tc similarities of less than 0.35 versus around 28,000 annotated dopaminergic, serotonergic and adrenergic ligands from the ChEMBL20 database<sup>27</sup>.

## Initial synthesis and testing

From the remaining top-ranking clusters, we synthesized 17 richly functionalized THPs. The selected primary amines **4** and  $\alpha,\beta$ -unsaturated carbonyls **5** were first condensed to provide  $\alpha,\beta$ -unsaturated imines **8** (Extended Data Fig. 1a). A one-pot reaction sequence then furnished THP subtypes ( $\pm$ )-**1** to ( $\pm$ )-**3** by Rh(I)-catalysed C–H addition of imine **8** to alkyne inputs **6** or **7** with in situ electrocyclization to give dihydropyridines ( $\pm$ )-**9** or ( $\pm$ )-**10**, respectively. THPs ( $\pm$ )-**1** to ( $\pm$ )-**3** were obtained by submitting dihydropyridines ( $\pm$ )-**9** or ( $\pm$ )-**10** to different reduction protocols without any work-up or isolation. To facilitate the synthesis of some initial compounds, and for later analogue synthesis (vide infra), a route was developed for the late-stage introduction of various R<sup>1</sup> substituents on the nitrogen of the THP core by preparing THPs ( $\pm$ )-**2** to ( $\pm$ )-**3** with a cleavable substituent on the nitrogen (Extended Data Fig. 1b). The synthesized THPs display a range of interesting functionalities and are well differentiated from the endogenous agonist, serotonin and from previously reported 5-HT<sub>2A</sub>R synthetic ligands.

The initial set of 17 synthesized THPs were tested in radioligand displacement assays versus the 5-HT<sub>2A</sub>R, 5-HT<sub>2B</sub>R and 5-HT<sub>2C</sub>R subtypes. This identified four molecules with inhibitory constant (K<sub>i</sub>) values ranging from 0.67  $\mu$ M to 3.9  $\mu$ M—a 24% hit rate (Fig. 2a,b). In functional assays at the three 5-HT<sub>2</sub>R subtypes, these four ligands exhibited either agonist or antagonist activity, with agonist activity ranging from 1.9  $\mu$ M to 3.0  $\mu$ M at 5-HT<sub>2B</sub>R (Fig. 2c and Extended Data Table 2).

Docked poses of the confirmed ligands suggested that all four interact with conserved binding-site residues, including a salt bridge between the tertiary amine of the THPs and Asp155<sup>3.32</sup>, a characteristic interaction in aminergic and certainly serotonergic<sup>28</sup> GPCRs (Fig. 2d). Several of the THPs were also predicted to hydrogen bond with Asn343<sup>6.55</sup> on TM6 and

the main chain of residues on the second extracellular loop (ECL2), and to form van der Waals interactions with residues on transmembrane helices 3, 5 and 6. As the 5-HT<sub>2A</sub>R and 5-HT<sub>2B</sub>R orthosteric binding sites are highly conserved, with only four residues varying between them<sup>15</sup>, we hypothesized that even THP ligands binding primarily at the 5-HT<sub>2B</sub>R subtype could be optimized to engage the 5-HT<sub>2A</sub>R.

## Structure-based optimization

We initially focused on synthesizing THP analogues that conserved the pyridine and pyrazole substituents at the C5 position, while varying the substituent on the THP nitrogen. This substitution site showed greater variability in the early ligands and is also straightforward to modify from the many available building blocks. Twenty analogues incorporating the pyridine ring at the C5 position were synthesized and assayed for binding, initially as racemates. Several had improved affinity, and even those analogues with reduced affinity provided useful insights into structure activity relationships. Although the 3-hydroxyoxetane functionality was developed as a carboxylic acid bioisostere<sup>29</sup>, the corresponding carboxylic acid analogue ( $\pm$ )-**30** had no activity against 5-HT<sub>2A</sub>R or 5-HT<sub>2B</sub>R (Supplementary Fig. 2a). However, the oxygen heteroatoms in the hydroxyoxetane do contribute to binding because the 1-methylcyclobutyl ( $\pm$ )-**31** and neopentyl ( $\pm$ )-**32** analogues had reduced affinity. The location of the basic pyridyl nitrogen is also important as established by the lack of activity of the pyridine regioisomer ( $\pm$ )-**33**.

The eight highest-affinity racemic analogues were separated by chiral high-performance liquid chromatography (HPLC) and tested for binding and functional activity as single enantiomers (Supplementary Table 2). As exemplified for (**R**)-**35** and (**S**)-**35**, strong chiral discrimination was generally observed for the binding of each pair of enantiomers to both 5-HT<sub>2A</sub>R and 5-HT<sub>2B</sub>R. Encouragingly, docking correctly predicted that the *S*-enantiomer would bind with greater affinity. Improved binding affinity and functional activity was observed when the methyl substituent present on the pyridyl ring was replaced by the isosteric but metabolically stable chloro substituent, as exemplified by (**R**)/(**S**)-**35** and (**R**)/(**S**)-**36**. Based on the incipient 5-HT<sub>2B</sub>R hit ( $\pm$ )-**28** (Extended Data Table 2), the pentyl substituent was introduced on the THP nitrogen of (**S**)-**37**, resulting in submicromolar agonist activity at 5-HT<sub>2A</sub>R, although still with around tenfold greater agonism of 5-HT<sub>2B</sub>R. Analogues with variable alkyl chain lengths and branching were low-nanomolar agonists of 5-HT<sub>2B</sub>R, but unfortunately did not improve agonist activity at 5-HT<sub>2A</sub>R.

The C5-pyrazole substituent is present in two of our four initial active ligands. To capitalize on this substituent, we revisited the 4.3-billion-compound virtual library with molecular masses of  $\leq 400$  amu. Library members with a Tc of >0.5 to initial hits ( $\pm$ )-**26** and ( $\pm$ )-**28** were docked to the 5-HT<sub>2A</sub>R orthosteric binding site and their poses were assessed for steric complementarity and for favourable interactions with binding-site residues. Although numerous substituents with diverse steric profiles and hydrogen bonding abilities were examined off the THP nitrogen (( $\pm$ )-**43** to ( $\pm$ )-**54**), in all cases, a binding affinity of >10  $\mu$ M was observed at 5-HT<sub>2A</sub>R (Supplementary Fig. 2b). We also experimented with introducing nitrogen substituents from the other initial hit compounds in analogues ( $\pm$ )-**55** and ( $\pm$ )-**56**, but found that these changes were unfavourable. The larger ethyl rather than a methyl substituent at either C3 (( $\pm$ )-**57**) or on the pyrazole nitrogen (( $\pm$ )-**58**) was not tolerated.

Searching the greater 4.3-billion-compound virtual library for similar compounds with heteroaryl groups to replace the pyrazole substituent proved to be more successful, with the azaindole substituent resulting in improved affinity and functional activity. A total of 14 azaindole analogues were separated and tested as single enantiomers, with most exhibiting partial or full agonism at 5-HT<sub>2A</sub>R (Supplementary Table 3). Small nitrogen substituents provided the greatest agonist activity

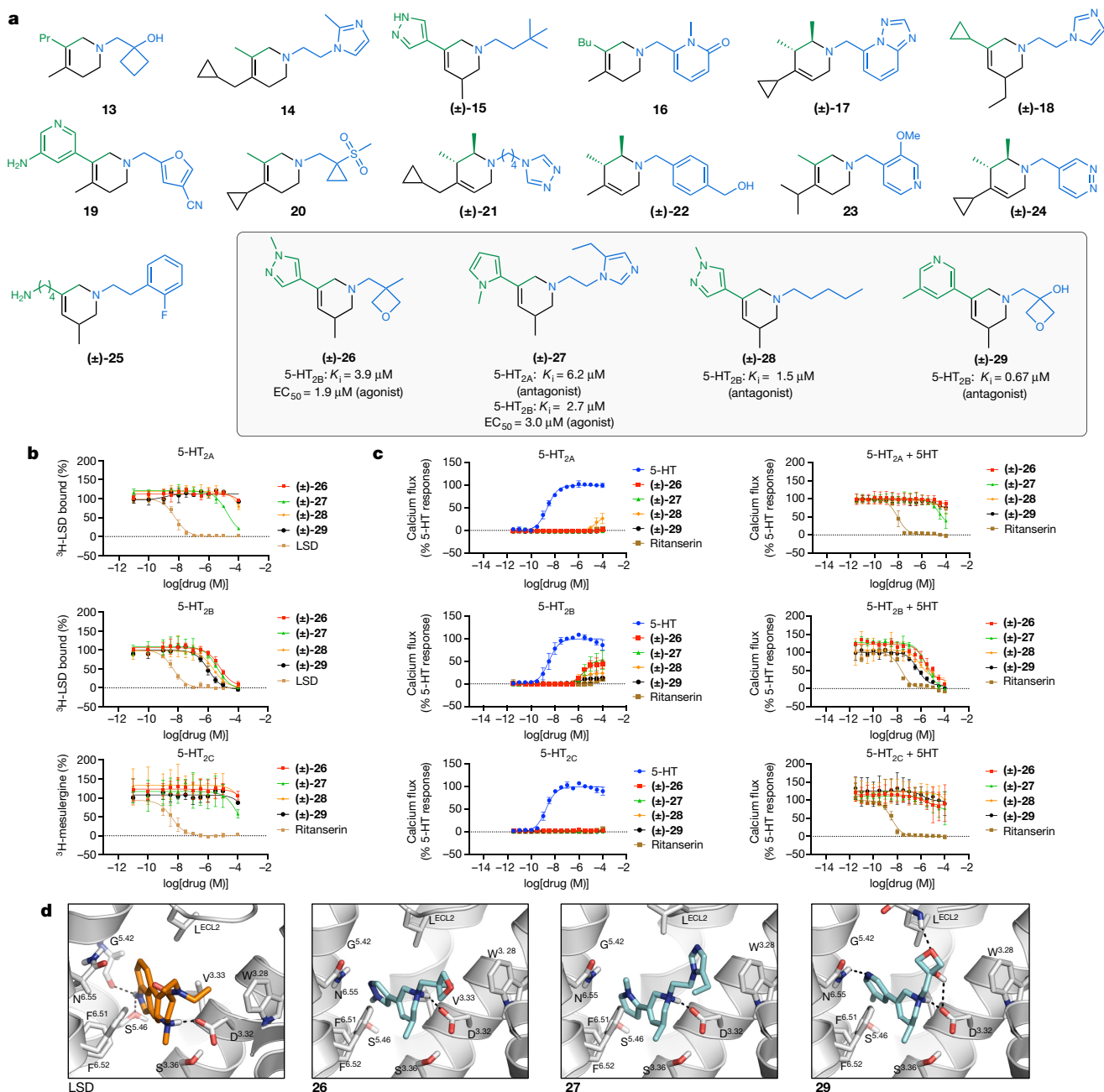


**Fig. 2 | A large-scale docking screen of a THP virtual library finds new 5-HT<sub>2R</sub> ligands.** **a**, The initial 17 compounds synthesized and assayed. Of these compounds, four had 5-HT<sub>2A</sub>R or 5-HT<sub>2B</sub>R activity (indicated by boxes). **b**, Binding of the four active compounds to human 5-HT<sub>2</sub>R<sub>s</sub> in radioligand-competition binding assays. Concentration–inhibition curves at 5-HT<sub>2A</sub>R and 5-HT<sub>2B</sub>R versus [<sup>3</sup>H]LSD, and at 5-HT<sub>2C</sub>R versus [<sup>3</sup>H]mesulergine. [<sup>3</sup>H]LSD and [<sup>3</sup>H]mesulergine concentrations of 0.5 nM and 1.0 nM were used, respectively. Dissociation constant (*K<sub>d</sub>*) values of [<sup>3</sup>H]LSD at human 5-HT<sub>2A</sub>R and 5-HT<sub>2B</sub>R

were 0.33 nM and 0.91 nM, respectively, and the *K<sub>d</sub>* value of [<sup>3</sup>H]mesulergine at human 5-HT<sub>2C</sub>R was 0.67 nM (refs. 20,77). LSD (5-HT<sub>2A</sub>R, 5-HT<sub>2B</sub>R) and ritanserin (5-HT<sub>2C</sub>R) were used as positive controls. **c**, Concentration–response curves of the four active compounds at stable 5-HT<sub>2A</sub>R, 5-HT<sub>2B</sub>R and 5-HT<sub>2C</sub>R-IN1 in Flp-In293 cell lines in Ca<sup>2+</sup> assays. For **b** and **c**, data are mean ± s.e.m. from *n* = 3 independent experiments. **d**, Docked poses of characteristic molecules compared with that of LSD. Ballesteros–Weinstein residue numbering is shown in superscript.

and led to the identification of 5-HT<sub>2A</sub>R strong partial agonists (**R**-69 and **R**-70 with 41 nM and 110 nM half-maximal effective concentration (EC<sub>50</sub>) values in a calcium flux assay, respectively (Fig. 3a–c). By contrast, introduction of the larger 2-(3-(2-methylpyrimidinyl)ethyl) nitrogen substituent provided a selective 5-HT<sub>2A</sub>R antagonist (**S**-65 with 59 nM activity (Fig. 3 and Supplementary Table 3). The partial agonists (**R**-69 and **R**-70) were structurally similar to the initial docking hits, including C5 placement of a heteroaromatic ring and the importance of both unsaturation and the C3 methyl substituent in the THP ring (see **71** and **72**).

### Target and functional selectivity

Selective activity on 5-HT<sub>2A</sub>R versus off-targets such as the closely related 5-HT<sub>2B</sub>R, other serotonin receptors—metabotropic but also ionotropic—and even transporters is important for usefulness as chemical probes and for therapeutic potential (for example, 5-HT<sub>2B</sub>R agonists can cause valvular heart disease)<sup>17</sup>. (**R**-69 had an agonist EC<sub>50</sub> of 190 nM versus 5-HT<sub>2B</sub>R, making it 4.6-fold selective for the 5-HT<sub>2A</sub>R, whereas (**R**-70 is 6.4-fold selective for 5-HT<sub>2A</sub>R versus 5-HT<sub>2B</sub>R (Fig. 3c); the two compounds were 29- to 51-fold selective versus 5-HT<sub>2C</sub>R. Against a panel

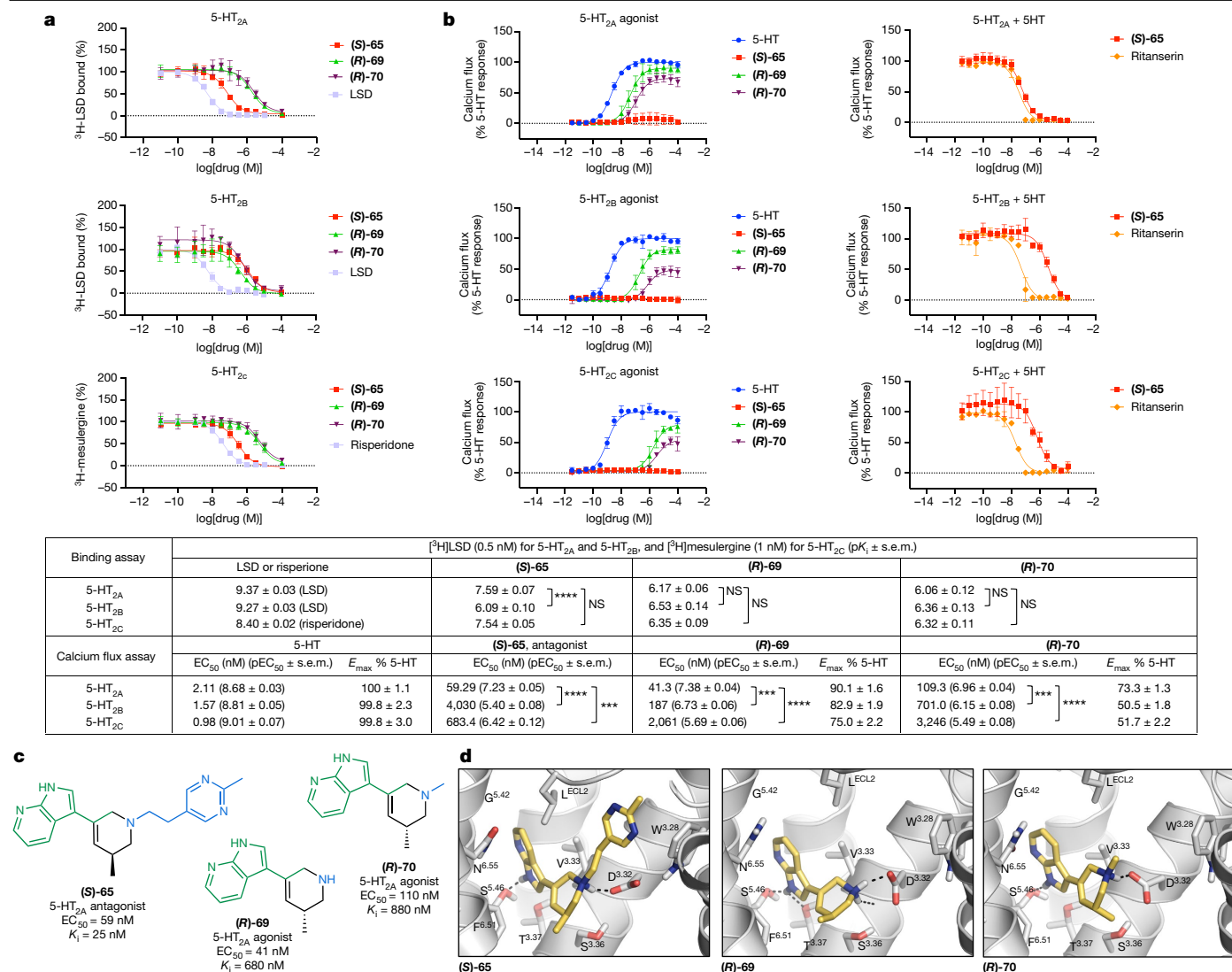


**Fig. 3 | Structure-guided discovery of 5-HT<sub>2A</sub> agonists and antagonists.** **a**, Dose–response competition binding assays of (S)-65, (R)-69 and (R)-70 against [<sup>3</sup>H]LSD for 5-HT<sub>2A</sub>R and 5-HT<sub>2B</sub>R, and [<sup>3</sup>H]mesulergine for 5-HT<sub>2C</sub>R. [<sup>3</sup>H]LSD and [<sup>3</sup>H]mesulergine concentrations of 0.3 nM and 1 nM were used, respectively. LSD (5-HT<sub>2A</sub>R, 5-HT<sub>2B</sub>R) and risperidone (5-HT<sub>2C</sub>R) were used as positive controls. **b**, Concentration–response curves of (S)-65, (R)-69 and (R)-70 at stable 5-HT<sub>2A</sub>R, 5-HT<sub>2B</sub>R and 5-HT<sub>2C</sub>R-INI in Flp-In293 cell lines in Ca<sup>2+</sup> assays. (R)-69 and (R)-70 are strong partial G<sub>q</sub> agonists, whereas (S)-65 acts as an antagonist. For **a** and **b**, data are mean ± s.e.m. from *n* = 3 independent

experiments. The pK<sub>i</sub> and EC<sub>50</sub> values between 5-HT<sub>2A</sub>R, 5-HT<sub>2B</sub>R and 5-HT<sub>2C</sub>R were compared using one-way analysis of variance (ANOVA) with Dunnett’s post-test; \**P* < 0.05, \*\**P* < 0.01, \*\*\**P* < 0.001, \*\*\*\**P* < 0.0001; NS, not significant. **c**, 2D structures and binding and functional affinities for the new ligands across the 5-HT<sub>2</sub>R subtypes. **d**, The docking poses of (S)-65 (left), (S)-69 (the better scoring enantiomer; middle) and (R)-70 (right). 5-HT<sub>2A</sub>R is shown in grey, the docked compounds are shown as capped sticks with carbons in yellow. Ballesteros–Weinstein residue numbering is shown in superscript.

of 318 other GPCRs in a β-arrestin-recruitment assay<sup>30</sup>, neither (R)-69 nor (R)-70 had measurable agonism, nor did either antagonize the hERG ion channel, a toxicology anti-target, up to 10 μM (Extended Data Fig. 2a–c). By ligand displacement, no substantial binding was measured at 45 other off-targets (Extended Data Table 3 and Supplementary Table 5). Although (R)-69 had modest (0.8 μM) activity for the serotonin transporter SERT, (R)-70 had no measurable activity, and neither compound was active versus the DAT or NET transporters. Compared with classic psychedelic 5-HT<sub>2A</sub>R agonists such as LSD, psilocin and DMT<sup>31</sup>, the new agonists are selective against most common serotonergic off-targets (Extended Data Fig. 2d–f). Although the EC<sub>50</sub> of even (R)-69 (41 nM) can seem modest, we note that it is within the range of many in vivo active 5HT<sub>2A</sub> receptors agonists, including mescaline (4 μM) psilocin (24 nM), LSD (6.4 nM) and lisuride (17 nM), while its selectivity versus 5HT<sub>2B</sub> and especially 5HT<sub>2C</sub> is substantially higher compared with these classic agonists. Meanwhile, the optimized THPs have unusually

high ligand efficiencies, reaching 0.6 kcal per heavy atom count (HAC), contributing to the high brain exposure achieved by the molecules and to their in vivo efficacy (discussed below).

In contrast to the psychedelic 5-HT<sub>2A</sub>R agonist LSD, which is arrestin-biased<sup>15,19,20,32</sup>, the new agonists were G-protein-biased, activating G<sub>q</sub> signalling at mid-nanomolar concentrations with high efficacy, whereas βArr2 recruitment was detectable only at higher concentrations. To quantify these differential kinetics, we calculated transduction coefficients at each time point for G<sub>q</sub> and βArr2 activities. (R)-69 and (R)-70 displayed stable differences in contrast to the other tested 5-HT<sub>2A</sub>R ligands, which had more variable patterns (Extended Data Fig. 3).

### Structure prediction and determination by cryo-EM

As the S-enantiomer docked better during hit optimization, we sought to refine the docked pose of (S)-69, as it would be important for further

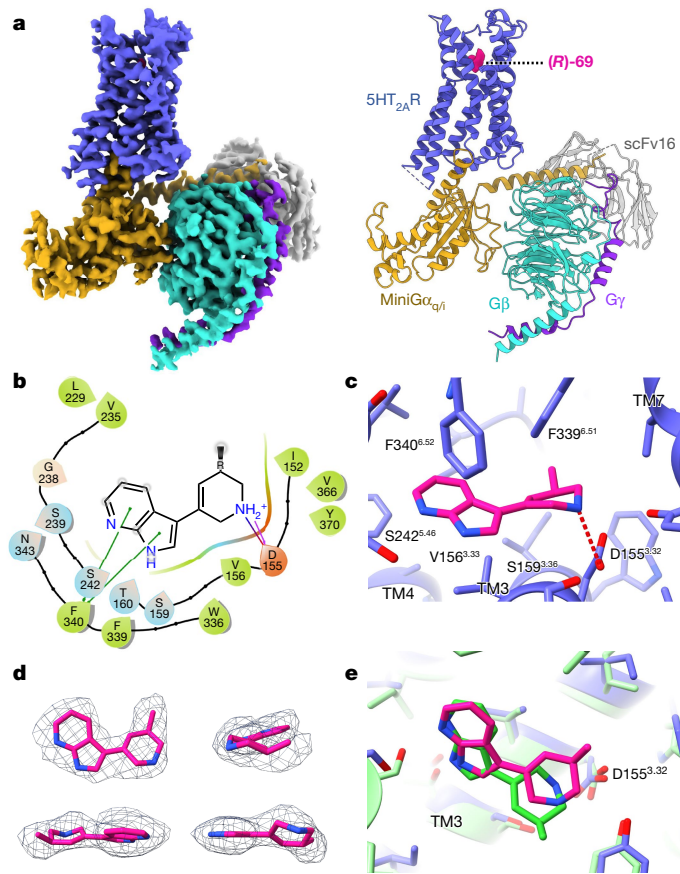


**Fig. 4 | The structure of 5-HT<sub>2A</sub>R bound to (R)-69 determined using cryo-EM.**

**a**, Overall cryo-EM map (left) and model (right) of 5-HT<sub>2A</sub>R bound to (R)-69 in a complex with miniG<sub>q/i</sub>. **b**, Schematic of ligand-specific interactions between (R)-69 and orthosteric residues of 5-HT<sub>2A</sub>R. A salt bridge with Asp155<sup>3,32</sup> is shown as a red dashed line. Colour code for residues and interactions: green, hydrophobic; blue, polar; red, negatively charged; grey, glycine. The solid green line shows the Pi–Pi stacking interaction. **c**, Specific residues in the binding pocket that interact with (R)-69 are shown as sticks and are labelled. (R)-69 is shown as magenta sticks. A salt bridge with Asp155<sup>3,32</sup> is shown as a red dashed line. **d**, Cryo-EM density for (R)-69. **e**, Comparison of the computationally predicted and experimentally resolved binding poses of (S)-69 and (R)-69, respectively. The cryo-EM structure in magenta is superposed on (S)-69 docked to the 5-HT<sub>2A</sub>R homology model in green. For **c** and **e**, Ballesteros–Weinstein residue numbering is shown in superscript.

optimization of this series. Starting with the homology model of 5-HT<sub>2A</sub>R used in the ligand discovery phase, 40 ligand poses were generated. These were clustered into six poses and used as starting points for 50 ns molecular dynamics (MD) simulations. Two stable poses emerged and were used to run retrospective free-energy perturbation (FEP)<sup>33</sup> for analogues of (S)-69, comparing these with experimentally measured binding affinities; the ligand–receptor complex of which the relative affinities by FEP corresponded most closely to those of the analogues within this series was chosen as the final predicted pose (Supplementary Fig. 3). The pose features a salt bridge with Asp155<sup>3,32</sup>, a hydrogen bond with Ser242<sup>5,46</sup> and packing interactions with Phe222<sup>6,52</sup>.

To template future compound optimization, understand activity at atomic resolution and test the predicted structures, we determined the structure of 5-HT<sub>2A</sub>R bound to (R)-69 using single-particle cryo-EM. We used our previously reported strategy<sup>15</sup> in which the 5-HT<sub>2A</sub>R–miniG<sub>q</sub> complex was formed from separately purified receptor in the presence of (R)-69 and miniG<sub>q</sub> heterotrimer and further stabilized through the binding of a single-chain variable fragment

(scFv16)<sup>34</sup>. We obtained the cryo-EM structure of the complex at a global nominal resolution of 3.4 Å (Fig. 4a, Extended Data Fig. 4 and Extended Data Table 4).

The high-quality cryo-EM density in the 5-HT<sub>2A</sub>R orthosteric site allowed for unambiguous modelling of (R)-69 (Fig. 4d), which was further confirmed through the GemSpot pipeline<sup>35</sup>. Interactions with the orthosteric site residues include the key salt bridge interaction with Asp155<sup>3,32</sup>, and a Pi–stacking interaction between the azaindole of (R)-69 and Phe340<sup>6,52</sup> (Fig. 4b,c). Multiple additional hydrophobic interactions, including Val156<sup>3,33</sup>, Val235<sup>5,39</sup>, Trp336<sup>6,48</sup> and Phe339<sup>6,51</sup>, also seem to have a role in (R)-69 binding. Although other polar interactions may be present in (R)-69 binding, no hydrogen-bond interaction was observed with the orthosteric site residues Ser239<sup>5,43</sup>, Ser242<sup>5,46</sup> or Ser159<sup>3,36</sup>, which are key for LSD and 25CN-NBOH (a *N*-benzyl phenethylamine full-agonist<sup>15</sup>) binding, respectively.

The superposition of the docked (S)-69 and experimental (R)-69-bound 5-HT<sub>2A</sub>R structures revealed good correspondence, with the azaindole groups superimposed almost identically (Fig. 4e). The cryo-EM structure shows that the (R)-69 THP ring adopts a slightly different conformation to the computationally predicted one, with the C3 methyl substituent pointing to the extracellular side of the binding pocket. Nonetheless, the key interaction between the THP ring amine and the Asp155<sup>3,32</sup> carboxylate is present as designed.

The cryo-EM structure of (R)-69-bound 5-HT<sub>2A</sub>R–miniG<sub>q/i</sub> informs comparisons with other 5-HT<sub>2A</sub>R structures (Extended Data Fig. 5). As with our previously described structure of 25CN-NBOH-bound 5-HT<sub>2A</sub>R in a complex with a G protein (PDB: 6WHA)<sup>15</sup>, reflecting the activated state of the receptor, the intracellular ends of TMS and TM6 in the (R)-69-bound 5-HT<sub>2A</sub>R–miniG<sub>q/i</sub> adopt an open conformation accommodating the binding of the G protein α-5 helix (Extended Data Fig. 5a). 5-HT<sub>2A</sub>R–miniG<sub>q/i</sub> interactions are almost identical to those described for 25CN-NBOH, supporting the importance of 5-HT<sub>2A</sub>R residues Asn107<sup>2,37</sup>, Asp172<sup>3,49</sup>, Asn317<sup>6,29</sup> and Asn384<sup>8,47</sup> in hydrogen bonding with Gα<sub>q</sub> residues Glu242<sup>HS,22</sup>, Tyr243<sup>HS,23</sup>, Gln237<sup>HS,17</sup> and Asn244<sup>HS,24</sup>. As was also seen in the other activated structures, in the (R)-69–5-HT<sub>2A</sub>R–miniG<sub>q/i</sub> complex, the residues Ala321<sup>6,33</sup>, Leu261<sup>5,65</sup>, Ile177<sup>3,54</sup>, Leu325<sup>6,37</sup> and Val324<sup>6,36</sup> of 5-HT<sub>2A</sub>R form a hydrophobic core with Leu236<sup>HS,16</sup>, Leu240<sup>HS,20</sup> and Leu245<sup>HS,25</sup> of Gα<sub>q</sub>. In the complex with (R)-69, as in the earlier activated structures, receptor stabilization by G-protein binding includes the rearrangement of ICL2 to a well-structured α-helix (Extended Data Fig. 5a).

In the (R)-69 complex, the ‘toggle switch’ residue Trp336<sup>6,48</sup> is in an ‘upward’ conformation that is closer to the inactive LSD-bound configuration (PDB: 6WGT)<sup>15</sup> versus the ‘downward’ configuration observed in the 25CN-NBOH-bound structure (due to the location of the 25CN-NBOH phenol moiety). Nonetheless, Trp336<sup>6,48</sup> is found at the same position in both active structures (Extended Data Fig. 5b) due to the opening of TM6 after G-protein binding with an identical subsequent conformation of the side chain of Phe332<sup>6,44</sup> in the PIF (Phe<sup>5,50</sup>–Ile<sup>3,40</sup>–Phe<sup>6,44</sup>) motif. The PIF motif is known to undergo conformational changes after receptor activation<sup>19</sup>. Notably, (R)-69 extends more towards TMS than LSD does in its complex with the inactive state of 5-HT<sub>2A</sub>R. As also observed for the 25CN-NBOH-bound structure, the (R)-69 complex displays an orthosteric binding pocket that is open to the extracellular side of the receptor (Extended Data Fig. 5c (top)), while it is more closed in the LSD-bound structure<sup>15</sup>. Interestingly, even though (R)-69 lacks a substituent binding towards the intracellular side of the pocket, a deeper extension of the pocket appears to open between TM3 and TM6 (Extended Data Fig. 5c (bottom)). Compared with newly determined X-ray structures of the classic agonists serotonin and psilocin<sup>36</sup>, which bind relatively high in the orthosteric site of the 5HT<sub>2A</sub>R, towards its cytoplasmic face, (R)-69 binds about two-rings deeper in the site, more closely engaging recognition residues such as Phe339, Phe340 and Ser242.

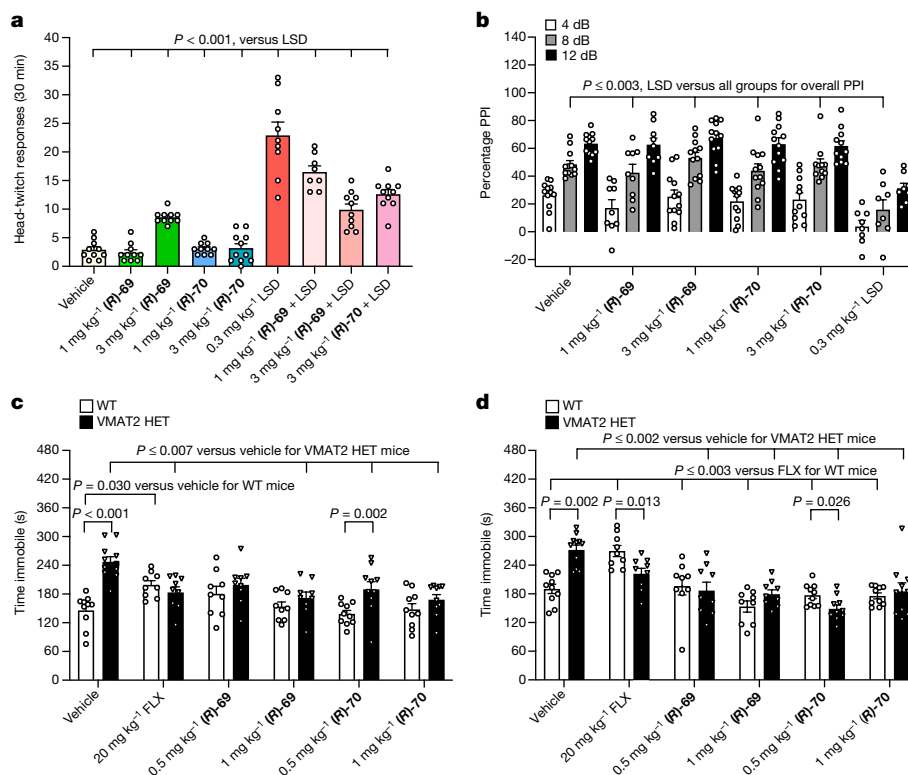


**Fig. 5 | HTRs, PPI responses and antidepressant-like actions of (R)-69 and (R)-70 in mice.** **a**, HTRs in C57BL/6J mice during the first 30 min after injection (i.p.) of vehicle, 1 or 3 mg kg<sup>-1</sup> (R)-69, 1 or 3 mg kg<sup>-1</sup> (R)-70, 0.3 mg kg<sup>-1</sup> LSD, 1 or 3 mg kg<sup>-1</sup> (R)-69 + 0.3 mg kg<sup>-1</sup> LSD, or 3 mg kg<sup>-1</sup> (R)-70 + 0.3 mg kg<sup>-1</sup> LSD. HTRs are low in the (R)-69 and (R)-70 groups, and they partially block the effects of LSD. **b**, PPI in C57BL/6J mice treated (i.p.) with vehicle, 1 or 3 mg kg<sup>-1</sup> (R)-69, 1 or 3 mg kg<sup>-1</sup> (R)-70, or LSD. PPI is unaffected by (R)-69 or (R)-70 relative to the vehicle and LSD disruption. **c**, **d**, Immobility in tail suspension at 30 min (c) and 24 h (d) after injection of wild-type (WT) and VMAT2 HET mice with a single injection (i.p.) of vehicle, 20 mg kg<sup>-1</sup> FLX, 0.5 or 1 mg kg<sup>-1</sup> (R)-69, or 0.5 or 1 mg kg<sup>-1</sup> (R)-70. Acute genotype differences were seen with vehicle and

0.5 mg kg<sup>-1</sup> (R)-70; at 24 h, the effects were present with vehicle, FLX and 0.5 mg kg<sup>-1</sup> (R)-70. In wild-type mice, immobility was enhanced by acute administration of FLX relative to the vehicle and, at 24 h, it was increased with FLX compared with all of the other groups. In VMAT2 HET mice, 30 min after administration, FLX, 1 mg kg<sup>-1</sup> (R)-69, and 0.5 and 1 mg kg<sup>-1</sup> (R)-70 reduce immobility; and, at 24 h, 0.5 and 1 mg kg<sup>-1</sup> (R)-69 and (R)-70 are efficacious compared with the vehicle. For **a–d**, data are mean  $\pm$  s.e.m. *n* values are provided in the Methods. Primary statistics are provided in Supplementary Table 4. For **a–d**, Bonferroni pairwise corrected *P* values were calculated across multiple comparisons for LSD, vehicle or FLX and the value closest to  $P < 0.05$  is shown (**a–d**), or within a single comparison between or within genotypes (**c** and **d**).

### Behavioural pharmacology

The potency and selectivity of (R)-69 and (R)-70 prompted us to investigate their biological activities, as drugs targeting 5-HT<sub>2A</sub>R as antagonists are prescribed for psychosis and other psychiatric indications<sup>37</sup>, whereas agonists can exert psychedelic, anxiolytic, anti-depressive and anti-drug abuse actions<sup>15,38</sup>. There is much interest in finding agonists that retain anti-depressive actions without the hallucinogenic effects of classic psychedelics such as LSD and psilocin. Encouragingly, both (R)-69 and (R)-70 had substantial brain permeability in mouse pharmacokinetic studies, with intraperitoneal (i.p.) injections of 10 mg kg<sup>-1</sup> leading to gross brain *C*<sub>max</sub> values of approximately 12  $\mu$ M and 35  $\mu$ M, plasma:brain ratios of 1.09 and 0.11, and brain half-lives of 111 min and 28.2 min for (R)-69 and (R)-70, respectively (Extended Data Fig. 6); exposures dosed at 1 mg kg<sup>-1</sup> remained substantial (Extended Data Fig. 6). These favourable CNS exposures prompted us to monitor head-twitch responses (HTRs)—classic indicators of 5-HT<sub>2A</sub>R engagement and psychedelic drug-like activity<sup>39,40</sup>. Different doses of both (R)-69 and (R)-70 induced very low levels of HTRs and, with the vehicle control, these values were significantly lower compared with those for the psychedelic LSD (Fig. 5a). Moreover, both (R)-69 and (R)-70 significantly blocked the HTRs induced by LSD itself. The level of inhibition of LSD-induced HTR by (R)-69 and (R)-70 is consistent with what one would expect for competition at the doses used, given the substantially greater

potency of LSD. As activation of the 5-HT<sub>2A</sub>R can lead to hallucinations<sup>41</sup>, partial blockade of LSD-induced HTRs with (R)-69 and (R)-70 further demonstrates that these compounds are unlikely to be psychedelic at these doses. In an additional test for psychedelic-like actions, (R)-69 and (R)-70 were found to exert no effects on prepulse inhibition (PPI) relative to LSD (Fig. 5b and Extended Data Fig. 7a,b).

Besides finding negligible psychedelic potentials for (R)-69 and (R)-70, we tested whether they would acutely stimulate or inhibit open field locomotion. Responses to both compounds were indistinguishable from the vehicle (Extended Data Fig. 8a,b). Moreover, both compounds blocked LSD-stimulated hyperlocomotion—further demonstrating the absence of motor-stimulating activities. Moreover, behavioural sensitization and conditioned place preference were not evident with the compounds relative to cocaine (Extended Data Fig. 8c, d). Thus, (R)-69 and (R)-70 do not possess locomotor-stimulating or reinforcing activity.

Psilocybin and LSD are reported to possess anxiolytic and antidepressant actions in cancer and other patients<sup>42–45</sup>. Accordingly, we tested effects of (R)-69 and/or (R)-70 in mouse genetic and learned helplessness models of depressive-like behaviours<sup>41</sup>. Some of these experiments used vesicular monoamine transporter 2 heterozygous (VMAT2 HET) mice, which present with motor-retardation in the open field, anhedonia-like behaviour to 1% and 1.5% sucrose solutions, enhanced learned helplessness and augmented stress-induced serum corticosterone levels compared with the wild-type controls. Similarly, in mutants,

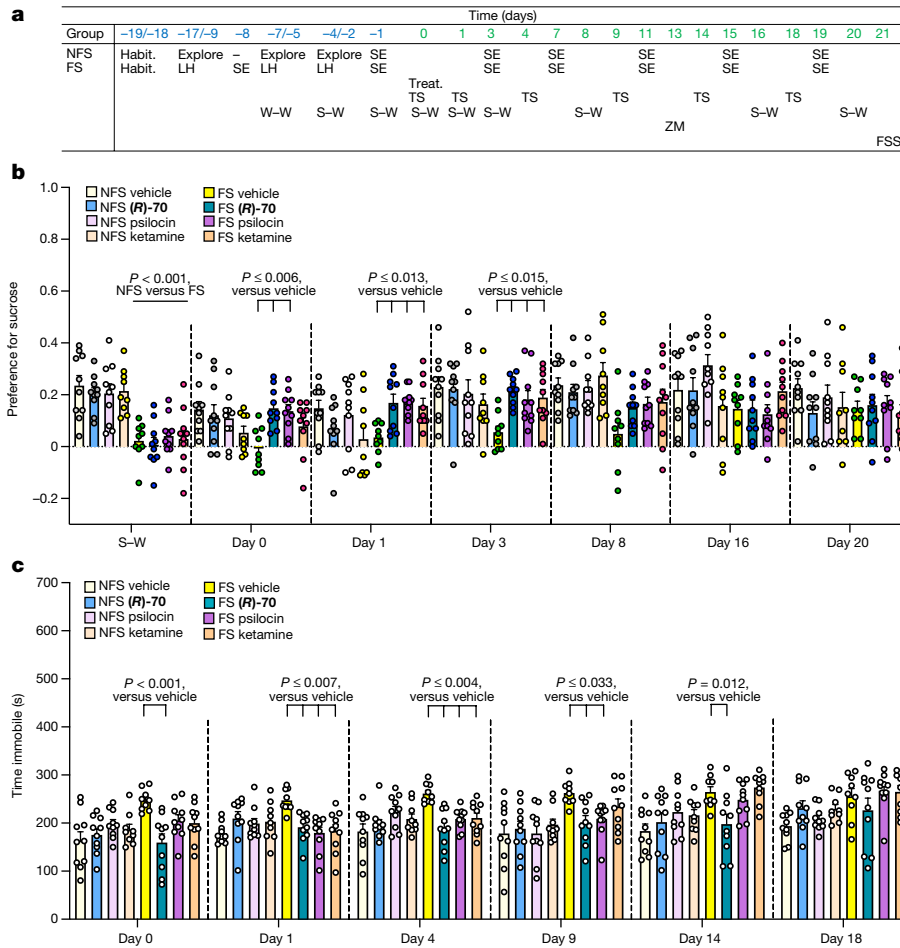


**Fig. 6 | Experimental design, sucrose preference and tail suspension for the learned helplessness experiment. a**, The experimental design. FSS, foot-shock sensitivity; habit., habituation; LH, learned helplessness training; treat., treatments (including vehicle, 1 mg kg<sup>-1</sup> (**R**)-70, 1 mg kg<sup>-1</sup> psilocin, 10 mg kg<sup>-1</sup> ketamine); TS, tail suspension; ZM, elevated zero maze. **b**, Sucrose preference in C57BL/6 mice assigned to the NFS and FS conditions and treated (i.p.) with vehicle, 1 mg kg<sup>-1</sup> (**R**)-70, 1 mg kg<sup>-1</sup> psilocin or 10 mg kg<sup>-1</sup> ketamine. During the initial sucrose–water (S–W) pairing, mice in the FS condition have a lower preference for sucrose compared with the NFS mice. Among the NFS mice, no treatment effects were found within days. By contrast, among FS mice, sucrose preference was reduced in the vehicle controls compared with the (**R**)-70 and psilocin groups on days 0, 1 and 3. The effects of ketamine were delayed

but become manifest on days 1 and 3. **c**, Tail suspension testing in the same mice. Times of immobility were low and stable across time in the NFS mice. In the FS condition, 30 min after treatment (day 0), immobility was high in the vehicle control relative to the (**R**)-70 group, and this effect persisted until day 14. Relative to the FS vehicle control, psilocin and ketamine showed efficacy on days 1 and 4, with the effects of psilocin lasting until day 9 after injection. For **b** and **c**, data are mean ± s.e.m. *n* values are provided in the Methods. Primary statistics are provided in Supplementary Table 4. For **b** and **c**, Bonferroni pairwise corrected *P* values were calculated across multiple comparisons to the vehicle within the FS condition and the closest value to *P* < 0.05 is shown, or within a single comparison to the vehicle (**b** and **c**) or condition (**b**).

immobility times are increased in the forced swim and tail suspension tests; these immobility times were normalized to those of the well-known antidepressants imipramine, fluoxetine (FLX), reboxetine and bupropion. Responses to (**R**)-69 and (**R**)-70 and several other drugs were examined 30 min and 24 h after administration in the VMAT2 HET mice and compared with wild-type mice (Fig. 5c,d). Examining the first paired columns (Fig. 5c,d), wild-type mice treated with vehicle had lower immobility times compared with VMAT2 HET mice both acutely and at 24 h, consistent with the depressive-like phenotype of these mutants (significance values between pairs are shown above the bars in all comparisons). Notably, the enhanced immobility of the VMAT2 HET mice was normalized to the acute administration of FLX, 1 mg kg<sup>-1</sup> (**R**)-69, or 0.5 or 1 mg kg<sup>-1</sup> (**R**)-70, and it remained at wild-type vehicle levels 24 h after administration for both doses of (**R**)-69 and (**R**)-70. Thus, in this mouse genetic model, both (**R**)-69 and (**R**)-70 possess antidepressant-like actions at least over 24 h.

To determine whether the antidepressant-like activities of (**R**)-69 and (**R**)-70 were mediated through 5-HT<sub>2A</sub>R or 5-HT<sub>2C</sub>R, we administered the

respective antagonists MDL 100907 and SB 242084. Unfortunately, relative to the vehicle control, we found that both antagonists decreased immobility on their own in VMAT2 HET mice, confounding the interpretation of this experiment (Extended Data Fig. 7c,d).

To further investigate the antidepressant actions of (**R**)-70, C57BL/6J mice were tested in a learned helplessness experiment (Fig. 6a). Note that these experiments were not conducted with (**R**)-69 owing to reagent limitations. Mice were assigned to foot-shock (FS) and non-FS (NFS) conditions and were given 16 days of training. Subsequently, the animals received a single administration (i.p.) of vehicle, 1 mg kg<sup>-1</sup> (**R**)-70, 1 mg kg<sup>-1</sup> psilocin or 10 mg kg<sup>-1</sup> ketamine, and sucrose preference responses, immobility times and escape behaviours were examined over time, with anxiety-like behaviours evaluated 13 days after injection. Before drug administration during the pairing of sucrose and water solutions (S–W pairing), FS mice showed a reduced sucrose preference compared with the NFS mice (Fig. 6b). Thus, FS mice exhibit depressive-like behaviour. After treatment (days 0–20) no significant effects were observed within days among the NFS mice. Crucially,



sucrose preference in FS mice was diminished in the vehicle controls versus the (**R**)-**70** and psilocin groups in which antidepressant-like effects were immediate (acute on day 0) and persisted over 3 days after injection. Thus, (**R**)-**70** and psilocin substantially increase sucrose preference among the FS mice. The corresponding effects of ketamine were not apparent until day 1, but were maintained until day 3. By day 8, the levels of sucrose preference in all of the groups were not statistically different. The reduced sucrose preference in FS mice was not due to decreased fluid intake, as they drank greater volumes of the sucrose solution and water compared with NFS mice before treatment, as well as until day 3 after injection; after day 8, the levels of intake were similar between the NFS and FS conditions (Extended Data Fig. 7e).

Relative to sucrose preference, responses to the treatments between and within the FS and NFS conditions were more robust in the tail suspension test. Here, immobility times in NFS-treated mice were comparable across the 18 test days (Fig. 6c). By contrast, under the FS condition, immobility times were high in vehicle controls relative to the (**R**)-**70** group and this persisted to day 14. Compared with the FS vehicle controls, psilocin and ketamine were efficacious on days 1 and 4, with the psilocin effects lasting to day 9 after injection. Thus, (**R**)-**70** appears to have antidepressant-like activities not only in sucrose preference but also in tail suspension that persisted over days after a single injection.

In addition to depressive-like responses, anxiety-like behaviour was examined. In the elevated zero maze, FS mice spent less time in the open areas compared with NFS mice (Extended Data Fig. 9a). Within the FS condition, vehicle-treated mice spent less time in the open areas compared with animals that were given (**R**)-**70**, psilocin or ketamine. Moreover, in FS mice, the latency to enter the open areas was increased, whereas motor activities were reduced (Extended Data Fig. 9b,c). Together, these findings suggest that the FS mice display anxiety-like behaviours and this is especially apparent in vehicle-treated FS mice.

A key aspect of learned helplessness is the mouse's performance in escape testing<sup>41</sup>. This behaviour was examined as the numbers of escapes and latency to escape just before treatment (day -1) (Extended Data Fig. 10a,b). Compared with NFS mice, both escape indices were substantially affected in FS mice and they persisted throughout the experiment (that is, until day 19); no treatment effects were noted within the NFS or FS conditions. Together, these results reveal that treatments at the assigned doses could not overcome the escape decrements in the FS condition. Moreover, this decrement in performance suggests that the FS mice may be presenting not only with depressive- and anxiety-like behaviours, but also with post-traumatic stress disorder-like responses. To determine whether the different conditions or treatments were differentially sensitive to FS, all of the mice were tested for reactivity to this noxious stimulus (Extended Data Fig. 10c). Responses in the FS and NFS animals were similar to the 0–0.3 mA stimuli; responses to the 0.1 mA to 0.3 mA foot shock were undifferentiated and higher than those to the 0 mA condition. No treatment effects were found. Thus, impairment in escape performance in FS mice cannot be attributed to differential sensitivities to FS.

## Discussion

Here we describe a structure-based computational screen of a bespoke, ultralarge virtual library of molecules to find functionally selective agonists with interesting in vitro and in vivo activities. Three observations merit particular emphasis. First, a virtual library of 75 million THPs furnished structures that were under-represented in a general-purpose make-on-demand library. More than 99% of the molecules in the THP library have no equivalent in the general-purpose library, and 96% represent different scaffolds. Docking this library prioritized molecules that are active against 5-HT<sub>2</sub> receptor subtypes, ultimately leading to potent 5-HT<sub>2A</sub>R agonists with unusual kinetics for G-protein signalling versus arrestin recruitment. Second, the cryo-EM structure of the 5-HT<sub>2A</sub>R-(**R**)-**69** complex confirms the predicted structure and templates future

optimization of this new scaffold. Third, the novelty of (**R**)-**69** and (**R**)-**70** was mirrored in the new biology that they conferred, leading to agonists without psychedelic drug-like and locomotor-stimulating actions, which are typical of classical 5-HT<sub>2A</sub>R receptor agonists like LSD and psilocin<sup>46</sup>, but with anxiolytic-like and strong antidepressant drug-like effects in mouse models.

There were certain caveats. Synthetically, the rapid synthesis of highly functionalized, readily diversified scaffolds depends on facile, convergent and functional-group-compatible syntheses, limiting the scaffolds suitable for specialized virtual libraries. While the initial docking hit rate for 5-HT<sub>2</sub>R subtypes was high (24%), the hit rate for 5-HT<sub>2A</sub>R in particular was lower. Although the 5-HT<sub>2A</sub>R-(**S**)-**69** complex was predicted with high fidelity to the subsequent cryo-EM structure (Fig. 4), this demanded extensive MD and FEP simulations<sup>33,47</sup>, in which docking alone and even pose stability by MD alone<sup>48</sup> were insufficient. Rather, it was the combination of stable MD geometries<sup>48</sup> with FEP based on those geometries that led to the correct prediction. The unusual phenotype of the new agonists—conferring antidepressant drug-like activity without apparent psychedelic-like activity—may reflect their unusual functional selectivity between G protein and βArr recruitment through the 5HT<sub>2A</sub> receptor. Admittedly, a role for off-targets, including other 5HT<sub>2</sub> subtypes, and even for active metabolites, cannot be excluded. Finally, although the behavioural activity of the new agonists suggests therapeutic potentials, the current molecules demand more exploration and optimization before they can be considered to be drug candidates.

These caveats should not obscure the central observations of this study. A virtual library of 75 million THPs explored a functionally congested scaffold that is under-represented in general unbiased make-on-demand libraries. Docking this virtual library prioritized molecules that well-complemented 5-HT<sub>2A</sub>R, and the optimization of these molecules led to strong partial agonists with distinct signalling kinetics. As 5-HT<sub>2A</sub>R agonists, these molecules are potential leads for the development of therapeutics against disorders that have withstood long-term treatment, including depression, anxiety and post-traumatic stress disorder. More generally, multiple synthetic strategies<sup>49</sup> and scaffolds may furnish specialized virtual libraries representing chemotypes that are unavailable among general make-on-demand libraries. Such focused libraries may illuminate receptors and pharmacologies that have to date been inaccessible to the community.

## Online content

Any methods, additional references, Nature Research reporting summaries, source data, extended data, supplementary information, acknowledgements, peer review information; details of author contributions and competing interests; and statements of data and code availability are available at <https://doi.org/10.1038/s41586-022-05258-z>.

- Gloriam, D. E. Bigger is better in virtual drug screens. *Nature* **566**, 193–194 (2019).
- Lyu, J. et al. Ultra-large library docking for discovering new chemotypes. *Nature* **566**, 224–229 (2019).
- Gorgulla, C. et al. An open-source drug discovery platform enables ultra-large virtual screens. *Nature* **580**, 663–668 (2020).
- Stein, R. M. et al. Virtual discovery of melatonin receptor ligands to modulate circadian rhythms. *Nature* **579**, 609–614 (2020).
- Duttwyler, S., Lu, C., Rheingold, A. L., Bergman, R. G. & Ellman, J. A. Highly diastereoselective synthesis of tetrahydropyridines by a C–H activation–cyclization–reduction cascade. *JACS* **134**, 4064–4067 (2012).
- Duttwyler, S. et al. Proton donor acidity controls selectivity in nonaromatic nitrogen heterocycle synthesis. *Science* **339**, 678–682 (2013).
- Ischay, M. A., Takase, M. K., Bergman, R. G. & Ellman, J. A. Unstabilized azomethine ylides for the stereoselective synthesis of substituted piperidines, tropanes, and azabicyclo[3.1.0] systems. *JACS* **135**, 2478–2481 (2013).
- Lovering, F., Bikker, J. & Humblet, C. Escape from flatland: increasing saturation as an approach to improving clinical success. *J. Med. Chem.* **52**, 6752–6756 (2009).
- Boström, J., Brown, D. G., Young, R. J. & Keserü, G. M. Expanding the medicinal chemistry synthetic toolbox. *Nat. Rev. Drug Discov.* **17**, 709–727 (2018).
- Sterling, T. & Irwin, J. J. ZINC 15—ligand discovery for everyone. *J. Chem. Inf. Model.* **55**, 2324–2337 (2015).

11. Oprea, T. I., Davis, A. M., Teague, S. J. & Leeson, P. D. Is there a difference between leads and drugs? A historical perspective. *J. Chem. Inf. Comput. Sci.* **41**, 1308–1315 (2001).
12. Berger, M., Gray, J. A. & Roth, B. L. The expanded biology of serotonin. *Annu. Rev. Med.* **60**, 355–366 (2009).
13. McCorvy, J. D. & Roth, B. L. Structure and function of serotonin G protein-coupled receptors. *Pharmacol. Ther.* **150**, 129–142 (2015).
14. Meltzer, H. Y. & Roth, B. L. Lorcaserin and pimavanserin: emerging selectivity of serotonin receptor subtype-targeted drugs. *J. Clin. Invest.* **123**, 4986–4991 (2013).
15. Kim, K. et al. Structure of a hallucinogen-activated Gq-coupled 5-HT<sub>2A</sub> serotonin receptor. *Cell* **182**, 1574–1588 (2020).
16. Carhart-Harris, R. et al. Trial of psilocybin versus escitalopram for depression. *N. Engl. J. Med.* **384**, 1402–1411 (2021).
17. Roth, B. L. Drugs and valvular heart disease. *N. Engl. J. Med.* **356**, 6–9 (2007).
18. Rothman, R. B. et al. Evidence for possible involvement of 5-HT<sub>2B</sub> receptors in the cardiac valvulopathy associated with fenfluramine and other serotonergic medications. *Circulation* **102**, 2836–2841 (2000).
19. Wacker, D. et al. Structural features for functional selectivity at serotonin receptors. *Science* **340**, 615–619 (2013).
20. Wacker, D. et al. Crystal structure of an LSD-Bound human serotonin receptor. *Cell* **168**, 377–389 (2017).
21. Andrade, R. et al. *IUPHAR/BPS Guide to Pharmacology* Vol. 2019 (4) (2019).
22. Mysinger, M. M., Carchia, M., Irwin, J. J. & Shoichet, B. K. Directory of useful decoys, enhanced (DUD-E): better ligands and decoys for better benchmarking. *J. Med. Chem.* **55**, 6582–6594 (2012).
23. Huang, X. P. et al. Allosteric ligands for the pharmacologically dark receptors GPR68 and GPR65. *Nature* **527**, 477–483 (2015).
24. Lansu, K. et al. In silico design of novel probes for the atypical opioid receptor MRGPRX2. *Nat. Chem. Biol.* **13**, 529–536 (2017).
25. Ballesteros, J. A. & Weinstein, H. in *Methods in Neurosciences* Vol. 25 (ed. Sealfon, S. C.) 366–428 (Academic, 1995).
26. Irwin, J. J. & Shoichet, B. K. Docking screens for novel ligands conferring new biology. *J. Med. Chem.* **59**, 4103–4120 (2016).
27. Bento, A. P. et al. The ChEMBL bioactivity database: an update. *Nucleic Acids Res.* **42**, D1083–D1090 (2014).
28. Xu, P. et al. Structural insights into the lipid and ligand regulation of serotonin receptors. *Nature* **592**, 469–473 (2021).
29. Lassalas, P. et al. Evaluation of oxetan-3-ol, thietan-3-ol, and derivatives thereof as bioisosteres of the carboxylic acid functional group. *ACS Med. Chem. Lett.* **8**, 864–868 (2017).
30. Kroeze, W. K. et al. PRESTO-Tango as an open-source resource for interrogation of the druggable human GPCRome. *Nat. Struct. Mol. Biol.* **22**, 362–369 (2015).
31. Ray, T. S. Psychedelics and the human receptorome. *PLoS ONE* **5**, e9019 (2010).
32. Rodriguez, R. M. et al. LSD-stimulated behaviors in mice require beta-arrestin 2 but not beta-arrestin 1. *Sci. Rep.* **11**, 17690 (2021).
33. Abel, R., Wang, L., Harder, E. D., Berne, B. J. & Friesner, R. A. Advancing drug discovery through enhanced free energy calculations. *Acc. Chem. Res.* **50**, 1625–1632 (2017).
34. Maeda, S. et al. Development of an antibody fragment that stabilizes GPCR/G-protein complexes. *Nat. Commun.* **9**, 3712 (2018).
35. Robertson, M. J., van Zundert, G. C. P., Borrelli, K. & Skiniotis, G. GemSpot: a pipeline for robust modeling of ligands into Cryo-EM maps. *Structure* **28**, 707–716 (2020).
36. Cao, D. et al. Structure-based discovery of nonhallucinogenic psychedelic analogs. *Science* **375**, 403–411 (2022).
37. Meltzer, H. Y. The role of serotonin in antipsychotic drug action. *Neuropsychopharmacology* **21**, 1065–1155 (1999).
38. Nutt, D., Erritzoe, D. & Carhart-Harris, R. Psychedelic psychiatry's brave new world. *Cell* **181**, 24–28 (2020).
39. Corne, S. J. & Pickering, R. W. A possible correlation between drug-induced hallucinations in man and a behavioural response in mice. *Psychopharmacologia* **11**, 65–78 (1967).
40. Woolley, D. W. Production of abnormal (Psychotic?) Behavior in mice with lysergic acid diethylamide, and its partial prevention with cholinergic drugs and serotonin. *Proc. Natl Acad. Sci. USA* **41**, 338–344 (1955).
41. Roth, B. L., Willins, D. L., Kristiansen, K. & Kroeze, W. K. Activation is hallucinogenic and antagonism is therapeutic: role of 5-HT<sub>2A</sub> receptors in atypical antipsychotic drug actions. *Neuroscientist* **5**, 254–262 (1999).
42. Gasser, P., Kirchner, K. & Passie, T. LSD-assisted psychotherapy for anxiety associated with a life-threatening disease: a qualitative study of acute and sustained subjective effects. *J. Psychopharmacol.* **29**, 57–68 (2015).
43. Goldberg, S. B., Pace, B. T., Nicholas, C. R., Raison, C. L. & Hutson, P. R. The experimental effects of psilocybin on symptoms of anxiety and depression: a meta-analysis. *Psychiatry Res.* **284**, 112749 (2020).
44. Grob, C. S. et al. Pilot study of psilocybin treatment for anxiety in patients with advanced-stage cancer. *Arch. Gen. Psychiatry* **68**, 71–78 (2011).
45. Ross, S. et al. Rapid and sustained symptom reduction following psilocybin treatment for anxiety and depression in patients with life-threatening cancer: a randomized controlled trial. *J. Psychopharmacol.* **30**, 1165–1180 (2016).
46. Shao, L. X. et al. Psilocybin induces rapid and persistent growth of dendritic spines in frontal cortex in vivo. *Neuron* **109**, 2535–2544.e4 (2021).
47. Jorgensen, W. L. Efficient drug lead discovery and optimization. *Acc. Chem. Res.* **42**, 724–733 (2009).
48. Cutrona, K. J., Newton, A. S., Krimmer, S. G., Tirado-Rives, J. & Jorgensen, W. L. Metadynamics as a postprocessing method for virtual screening with application to the pseudokinase domain of JAK2. *J. Chem. Inf. Model.* **60**, 4403–4415 (2020).
49. Saper, N. I. et al. Nickel-catalysed anti-Markovnikov hydroarylation of unactivated alkenes with unactivated arenes facilitated by non-covalent interactions. *Nat. Chem.* **12**, 276–283 (2020).

**Publisher's note** Springer Nature remains neutral with regard to jurisdictional claims in published maps and institutional affiliations.

Springer Nature or its licensor holds exclusive rights to this article under a publishing agreement with the author(s) or other rightsholder(s); author self-archiving of the accepted manuscript version of this article is solely governed by the terms of such publishing agreement and applicable law.

© The Author(s), under exclusive licence to Springer Nature Limited 2022, corrected publication 2022

## Methods

## THP virtual library generation

The THP libraries were created as described below.

**Reagent selection.** We searched ZINC for commercially available building blocks to find reagents of which we could purchase 250 mg for under US\$250, filtering out molecules with incompatible functional groups. For example, molecules containing alkyne moieties in the amines, anilines or propenal reagents were eliminated. These compound lists were then manually curated for compatibility with the reaction scheme. We found 1,848 anilines, 276 trimethylsilylalkynes, 25 tertiary alkynes and 541 non-tertiary alkynes, 147 propenaldehydes, 283 propenals and 1,890 alkyl-amines. We capped the molecular mass to produce lead-like compounds as follows: TMS alkynes, 222 g mol<sup>-1</sup>; propanals and propenaldehydes, 160 g mol<sup>-1</sup>; alkyl amines, anilines and alkynes, 150 g mol<sup>-1</sup>.

**Reactions.** A list of the reaction SMARTs used for the reactions is provided in Supplementary Table 1. We used RDKit v.106\_03 for all manipulations. We generated molecules and filtered the list to remove molecules larger than 400 g mol<sup>-1</sup> and with a calculated log[P] > 3.5.

**3D building.** We built the libraries for docking as described for ZINC15<sup>10</sup>.

## Homology modelling

A homology model of the 5-HT<sub>2A</sub>R was calculated using the crystal structure of 5-HT<sub>2B</sub>R in complex with LSD as the template (PDB: 5TVN chain A)<sup>20</sup>. Sequence alignment for construction of 5-HT<sub>2A</sub>R homology models was generated with PROMALS3D<sup>50</sup>, using sequences of the human 5-HT<sub>2A</sub>R (UniProt: P28223), 5-HT<sub>2B</sub>R (UniProt: P41595), as well as sequences of all available 5-HT<sub>2B</sub>R X-ray structures (PDB: 4IB4 (chain A)<sup>19</sup>, 4NC3 (chain A)<sup>51</sup> and the 5-HT<sub>2B</sub>R–LSD complex (5TVN, chain A)<sup>20</sup>). The alignment was manually edited to remove the amino and carboxy termini that extended past the template structure, and to remove the engineered apocytochrome b562 RIL (BRIL) from the template and the corresponding residues in ICL3 of 5-HT<sub>2A</sub>R. On the basis of this alignment, 1,000 homology models were built using MODELER-9v15<sup>52</sup>. LSD was retained in the modelling to ensure a ligand-competent orthosteric site. Models were evaluated using DOCK3.7<sup>53</sup> for their ability to enrich known 5-HT<sub>2A</sub>R ligands over property-matched decoys in docking to the orthosteric binding site (below). Decoy molecules share the physical properties of known ligands, but are topologically distinct from them and they are therefore unlikely to bind, thus controlling the enrichment of molecules by physical properties alone. Thirty-four known ligands with molecular masses of <350 amu were extracted from the IUPHAR database<sup>54</sup>, and 1,899 property-matched decoys were generated using the DUD-E server<sup>22</sup>. The models were ranked by their adjusted logAUC<sup>22</sup> and by an enrichment factor at 1% of the docked database (EF<sub>1%</sub>). Models also had to reproduce the crystallographic pose of LSD in the template structure and form key interactions with the receptor, such as the observed salt bridge with Asp<sup>3.32</sup>. The best scoring model by ligand enrichment was further optimized through minimization with the AMBER and the GAFF force fields, the latter supplemented with AMIBCC charges<sup>55</sup>. The integrity of the minimized model was assessed by redocking the known ligands and decoy molecules and recalculating enrichment factors.

## Library docking and selection of potential ligands for synthesis and testing

The modelled orthosteric site of the 5-HT<sub>2A</sub>R model was screened against the 75 million THP library using DOCK3.7<sup>53</sup>. Parenthetically, DOCK3.7 places presampled ligand conformations into binding sites by superimposing ligand atoms on pseudoatoms (spheres) in the site. These pseudoatoms represent favourable positions for individual

ligand atoms. Here, 45 matching spheres were used, drawn from the docked pose of LSD. The docked ligands were scored by summing receptor–ligand electrostatic and van der Waals interaction energies and corrected for context-dependent ligand desolvation<sup>56,57</sup>. Receptor structures were protonated using Reduce<sup>58</sup>. Partial charges from the united-atom AMBER<sup>55</sup> force field were used for all receptor atoms. Potential energy grids for the different energy terms of the scoring function were precalculated using AMBER<sup>55</sup> for the van der Waals term and the Poisson–Boltzmann method QNIFFT<sup>59,60</sup> for electrostatics. Context-dependent ligand desolvation was calculated using an adaptation of the generalized Born method<sup>56</sup>. Ligands were protonated with Marvin (v.15.11.23.0, ChemAxon, 2015; <https://www.chemaxon.com>) at pH 7.4. Each protomer was rendered into 3D using Corina (v.3.6.0026, Molecular Networks; <https://www.mn-am.com/products/corina>), and conformationally sampled using Omega (v.2.5.1.4, OpenEye Scientific Software; <https://www.eyesopen.com/omega>). Ligand atomic charges and initial desolvation energies were calculated as described previously<sup>10</sup>. In the docking screen, each library molecule was sampled in approximately 23,000 orientations and, on average, 92 conformations. Overall, about 7.46 trillion complexes were sampled and scored; this took 8,698 core hours—or under 9 h of wall-clock time over 1,000 cores. Finally, the best scoring configuration for each docked molecule was relaxed by rigid-body minimization. Over 5 million molecules successfully docked, with ~880,000 receiving an energy score of ~30 kcal mol<sup>-1</sup> or better (lower).

Once the screen was completed, the top 300,000 ranked molecules were clustered by the ECFP4-based Tc of 0.5 to reduce redundancy. The best-scoring member was used to represent each of the resulting 14,959 clusters. The 4,000 top-ranking cluster heads were manually inspected for favourable geometry and interactions in Chimera<sup>61</sup>. Topologically diverse molecules that adopted favourable geometries and formed specific interactions with binding-site residues, such as a charge interaction with Asp155<sup>3,32</sup>, were prioritized. A total of 205 compounds were selected. These were filtered for novelty by calculating ECFP4-based Tc values against around 28,000 aminergic ligands (acting at serotonin, dopamine and adrenergic receptors) extracted from the ChEMBL20 database<sup>27</sup>. Molecules with Tc < 0.35 to these aminergic ligands were considered to be topologically dissimilar and passed this filter. Ultimately, 30 compounds were chosen for synthesis and experimental testing, 17 of which were successfully synthesized.

**(R)-69 binding pose refinement with MD and retrospective FEP**

The 5-HT<sub>2A</sub>R homology model structure was prepared using the Protein Preparation Wizard (Maestro, Schrodinger) using the default protocol, and protonation states for histidine, glutamic and aspartic acid residues were predicted by PROPKa<sup>62</sup> at a pH of 7.4. **(R)-69** was docked to the prepared structure through Glide SP and Induced Fit Docking (IFD) (Schrodinger). By enforcing hydrogen bond interactions to Asp155<sup>3,32</sup>, three poses were generated from each program and were processed for MD using Desmond.

The Force Field Builder<sup>33</sup> was used to parametrize missing dihedrals of **(R)-69**. Each pose of **(R)-69** together with the prepared receptor structure was then embedded in a POPC membrane, solvated and had Na<sup>+</sup> Cl<sup>-</sup> ions added to a 0.15 mM concentration. The MD systems were equilibrated for 100 ps of Brownian NVT at 10 K with restraints on all of the solute's heavy atoms, followed by 100 ps of Brownian NPT at 50 K and 200 ps of NPγT at 50 K. The system was then heated from 100 K to 300 K over 300 ps of NPγT ensemble with gradual release of restraints. A final NVT unrestrained was run for 200 ps. The production runs were sampled for 50 ns of unrestrained NPγT ensemble at 298 K. Trajectories from the production run were analysed using Simulation Interaction Diagram for RMSD, RMSF, protein–ligand interactions and ligand torsional profile.

FEP calculations were performed using FEP+ (Schrodinger)<sup>63</sup> on **(R)-69** and 19 analogues. Missing torsional parameters for the ligands were

refitted using Force Field Builder<sup>33</sup>. Glide SP docking with tight core constraint was used to align ligands to (**R**)-**69** of the equilibrated system. A perturbation map was then built using cyclohexenamine as the custom core. Perturbations in complex and in solvent were sampled in the NPyT ensemble for 10 ns, and the perturbation map was analysed using FEP+.

### THP synthesis

Compounds were synthesized as depicted in Extended Data Fig. 1. THPs ( $\pm$ )-**1** to ( $\pm$ )-**3** were obtained through a one-pot reaction sequence from imines **8** and alkynes **6** or **7** according to previously described procedures<sup>5–7</sup> (Extended Data Fig. 1a). All imines were freshly prepared from amines **4** and  $\alpha,\beta$ -unsaturated carbonyls **5**. Select THP compounds were synthesized in two additional steps when the late-stage introduction of various R<sup>1</sup> substituents on the nitrogen of the THP core was desired (Extended Data Fig. 1b). Starting inputs **4–7** that were prohibitively expensive or that had long delivery times were also synthesized (details for relevant building blocks are outlined in Supplementary Data 1). The final products were purified using silica gel chromatography, and enantiomerically pure compounds were obtained using chiral HPLC. Identity and purity were confirmed by <sup>1</sup>H and <sup>13</sup>C nuclear magnetic resonance (NMR) and high-resolution mass spectrometry. See Supplementary Data 1 for detailed synthetic procedures, analytical data, NMR spectra and, when appropriate, chiral HPLC traces to demonstrate enantiomeric purity for all of the final products listed in Extended Data Table 2 and Supplementary Tables 2 and 3.

### Radioligand-binding assay

HEK293T cells were purchased from the American Type Culture Collection (ATCC, CRL-11268). HEK293T cells were authenticated by the supplier (ATCC) using morphology and growth characteristics and STR profiling, and tested negative for mycoplasma infection. Competitive binding assays were performed using membrane preparations from HEK293T cells transiently expressing 5-HT<sub>2A</sub>R, 5-HT<sub>2B</sub>R and 5-HT<sub>2C</sub>R. Binding assays were run in 96-well plates in standard binding buffer (50 mM Tris, 0.1 mM EDTA, 10 mM MgCl<sub>2</sub>, 0.1% BSA, 0.01% ascorbic acid, pH 7.4). A total of 50  $\mu$ l of each of <sup>3</sup>H-LSD (final 0.5 nM) for 5-HT<sub>2A</sub>R and 5-HT<sub>2B</sub>R, and <sup>3</sup>H-mesulergine (final 1 nM) for 5-HT<sub>2C</sub>R, drug solution (3 $\times$ ) and homogeneous 5-HT<sub>2A/2B/2C</sub>R membrane solutions were incubated in 96-well plates in standard binding buffer. The reaction was incubated for 2 h at room temperature in the dark and terminated by rapid vacuum filtration onto chilled 0.3% PEI-soaked GHF/A filters followed by three quick washes with cold washing buffer (50 mM Tris HCl, pH 7.4) and read. The results were analysed using the equation ‘one-site fit Ki’ in GraphPad Prism v.9.0.

### Calcium flux assay

Stable cell lines for 5-HT<sub>2A</sub>R, 5-HT<sub>2B</sub>R and 5-HT<sub>2C</sub>R were generated using the Flp-In 293 T-Rex tetracycline-inducible system (Invitrogen). Tetracycline-induced cells were seeded in 384-well poly-L-lysine plates at a density of 10,000 cells per well in DMEM containing 1% dialysed FBS at least 16–24 h before the calcium flux assay. On the day of the assay, cells were incubated (20  $\mu$ l per well) for 1 h at 37 °C with Fluo-4 Direct dye (Invitrogen) reconstituted in FLIPR buffer (1 $\times$  HBSS, 2.5 mM probenecid and 20 mM HEPES, pH 7.4). After dye loading, cells were placed in a FLIPR<sup>TETRA</sup> fluorescence imaging plate reader (Molecular Dynamics). Drug dilutions were prepared at 3 $\times$  final concentration in drug buffer (1 $\times$  HBSS, 20 mM HEPES, 0.1% BSA, 0.01% ascorbic acid, pH 7.4), aliquoted into 384-well plates, and placed in the FLIPR<sup>TETRA</sup> for drug stimulation. The fluidics module and plate reader of the FLIPR<sup>TETRA</sup> were programmed to read baseline fluorescence for 10 s (1 read per s), then 10  $\mu$ l of drug per well was added and read for 5 min (1 read per s). The fluorescence in each well was normalized to the average of the first 10 reads (that is, the baseline fluorescence). The maximum-fold increase, which occurred within the first 60 s after drug addition, was

then determined and the fold change over baseline was plotted as a function of drug concentration. Data were normalized to percentage 5-HT stimulation and analysed using ‘log(agonist) versus response’ in GraphPad Prism v.9.0.

### BRET assay

For 5-HT<sub>2A</sub>R-, 5-HT<sub>2B</sub>R- and 5-HT<sub>2C</sub>R-mediated activation of G proteins, HEK293T cells were plated either into six-well dishes containing 700,000–800,000 cells per well or into 10 cm dishes at approximately 7–8 million cells per dish. Cells were transfected 2–4 h later, using a 1:1:1:1 ratio of the receptor:G $\alpha$ RLuc8:G $\beta$ :G $\gamma$ GFP DNA<sup>64</sup>. Transit 2020 (Mirus biosciences) was used to complex the DNA at a ratio of 3  $\mu$ l Transit per  $\mu$ g DNA in OptiMEM (Gibco) at a concentration of 10 ng DNA per  $\mu$ l OptiMEM. The next day, the cells were collected from the plate using Versene (0.1 M PBS + 0.5 mM EDTA, pH 7.4), and plated into poly-D-lysine-coated 96-well white assay plates (Greiner) at a density of 25,000–50,000 cells per well. One day after plating in 96-well plates, white backings (Perkin Elmer) were applied to the clear bottoms of the plate, and the medium was carefully aspirated and replaced with 60  $\mu$ l buffer (1 $\times$  HBBS, 20 mM HEPES, pH 7.4), incubated for 10 min at 37 °C and incubated again for 10 min but at room temperature. The buffer was carefully aspirated and replaced with 50  $\mu$ M coelenterazine 400a (Nanolight Technology) in 60  $\mu$ l buffer (1 $\times$  HBSS, 20 mM HEPES, pH 7.4). After a 5 min equilibration period, cells were treated with 30  $\mu$ l of 3 $\times$  final concentration in drug buffer (1 $\times$  HBSS, 20 mM HEPES, 0.1% BSA, 0.01% ascorbic acid, pH 7.4) for an additional 5 min. Plates were read in a LB940 Mithras plate reader (Berthold Technologies) with 395 nm (RLuc8-coelenterazine 400a) and 510 nm (GFP2) emission filters, at 1 s integration times. Plates were read six times, and measurements from the sixth read were used in all analyses. The bioluminescence resonance energy transfer (BRET) ratio represents the ratio of the GFP2 emission to rLuc8 emission. Data were normalized to percentage 5-HT stimulation and analysed using nonlinear regression ‘log(agonist) versus response’ in GraphPad Prism v.9.0.

To measure 5-HT<sub>2A</sub>R-, 5-HT<sub>2B</sub>R- and 5-HT<sub>2C</sub>R-mediated  $\beta$ -arrestin-2 recruitment, HEK293T cells were co-transfected at a 1:5 ratio with human 5-HT<sub>2A/B/C</sub>R containing C-terminal *Renilla* luciferase (RLuc8) and Venus-tagged N-terminal  $\beta$ -arrestin-2. After at least 16 h, transfected cells were plated in poly-L-lysine-coated 96-well white clear-bottom cell culture plates in plating medium (DMEM + 1% dialysed FBS) at a density of 25,000–50,000 cells in 200  $\mu$ l per well and incubated overnight. The next day, media were decanted and cells were washed twice with 60  $\mu$ l drug buffer (1 $\times$  HBSS, 20 mM HEPES, 0.1% BSA, 0.01% ascorbic acid, pH 7.4), then 60  $\mu$ l of drug buffer was added per well. For kinetic experiments, plates were incubated at 37 °C at least 20 min before receiving drug stimulation. Next, 30  $\mu$ l of drug (3 $\times$ ) was added per well and incubated for the designated time points. Before reading, 10  $\mu$ l of the RLuc substrate, coelenterazine h (Promega, 5  $\mu$ M final concentration) was added per well, incubated for an additional 5 min to allow for substrate diffusion, and the plates were immediately read for both luminescence at 485 nm and fluorescent eYFP emission at 530 nm for 1 s per well using the Mithras LB940 multimode microplate reader. The ratio of eYFP/RLuc was calculated per well and the net BRET ratio was calculated by subtracting the eYFP/RLuc per well from the eYFP/RLuc ratio in wells without Venus- $\beta$ -arrestin-2 present. Data were normalized to percentage 5-HT stimulation and analysed using nonlinear regression ‘log(agonist) versus response’ in GraphPad Prism v.9.0.

### GPCRome screen using PRESTO-Tango

Screening of compounds using the PRESTO-Tango GPCRome was accomplished using previously described methods with several modifications<sup>65</sup>. Confluent HTLA cells were passaged and subsequently plated in white 384-well clear bottom plates (Greiner) in DMEM (Sigma-Aldrich) with 1% dialysed FBS and 10 U ml<sup>-1</sup> penicillin-streptomycin (Gibco). After incubating at 37 °C and 5% CO<sub>2</sub> for 18 h, the cells

## Article

were transfected using PEI (Sigma-Aldrich) using an in-plate adapted method<sup>65</sup>. In brief, 22 ng per well of PRESTO-Tango GPCR DNAs were resuspended in OptiMEM (Gibco) and hybridized with PEI before dilution and distribution into 384-well plates and subsequent addition to cells. As an experimental control, dopamine receptor D2 was transfected in every plate. After overnight incubation, drugs diluted in DMEM with 1% dialysed FBS were added to cells without replacement of the medium, and medium alone was added for basal signals. For the tested compounds, a final concentration of 3  $\mu\text{M}$  was used. Dopamine receptor D2 assay controls were activated with 0.1 mM quinpirole in 16 replicate wells. The remaining steps of the PRESTO-Tango protocol were followed as previously described<sup>65</sup>. The results were presented in the form of fold change over basal for each receptor and plotted in GraphPad Prism.

### Formation of 5-HT<sub>2A</sub>R–miniG<sub>q/i</sub> heterotrimer and scFv16

The Bac-to-Bac Baculovirus Expression System (Invitrogen) was used to generate high-titre recombinant baculovirus (>10<sup>9</sup> viral particles per ml), expressed in sf9 cells, and the proteins 5-HT<sub>2A</sub>R, miniG<sub>q/i</sub>/ $\beta_1/\gamma_2$ , and scFv16 were purified. For purification of 5-HT<sub>2A</sub>R, thawed insect cell membranes were disrupted in a hypotonic buffer containing 10 mM HEPES (pH 7.5), 10 mM MgCl<sub>2</sub>, 20 mM KCl and protease inhibitors containing 500  $\mu\text{M}$  AEBF, 1  $\mu\text{M}$  E-64, 1  $\mu\text{M}$  leupeptin and 0.15  $\mu\text{M}$  aprotinin. Subsequently, soluble and membrane-associated proteins were removed in a high-osmotic buffer containing 10 mM HEPES (pH 7.5), 1,000 mM NaCl, 10 mM MgCl<sub>2</sub> and 20 mM KCl. Purified membranes were incubated in the presence of ligand, 25  $\mu\text{M}$  (**R**)-**69** and protease inhibitor cocktail at 4 °C for 2 h. The membranes were incubated with 2.0 mg ml<sup>-1</sup> iodoacetamide (Sigma-Aldrich) for 30 min and were solubilized in the buffer containing 50 mM HEPES (pH 7.5), 1% (w/v) n-dodecyl- $\beta$ -D-maltopyranoside (DDM, Anatrace), 0.2% (w/v) cholesterol hemisuccinate (CHS, Sigma-Aldrich) and 150 mM NaCl, at 4 °C for 2 h. Solubilized 5-HT<sub>2A</sub>R proteins in the supernatants were isolated by ultracentrifugation at 40,000g at 4 °C for 50 min, and then incubated at 4 °C overnight with TALON IMAC resin (Clontech), 800 mM NaCl and 20 mM imidazole as the final buffer concentrations. The resin was washed with 10 column volumes of buffer I containing 50 mM HEPES (pH 7.5), 0.1% (w/v) DDM, 0.02% (w/v) CHS, 800 mM NaCl, 10% (v/v) glycerol, 20 mM imidazole and 50  $\mu\text{M}$  (**R**)-**69** and with 10 column volumes of buffer II consisting of 50 mM HEPES (pH 7.5), 0.05% (w/v) DDM, 0.01% (w/v) CHS, 500 mM NaCl, 10% (v/v) glycerol and 50  $\mu\text{M}$  (**R**)-**69**. The protein was eluted using 3 column volumes of buffer containing 50 mM HEPES (pH 7.5), 0.05% (w/v) DDM, 0.01% (w/v) CHS, 500 mM NaCl, 10% glycerol, 250 mM imidazole and 50  $\mu\text{M}$  (**R**)-**69**. The sample was concentrated in the Vivaspin 20 concentrator with a molecular mass cut-off of 100 kDa (Satorius Stedim) to 500  $\mu\text{l}$ . This volume of 5-HT<sub>2A</sub>R protein sample was applied to PD MiniTrap G-25 columns (GE Healthcare) to remove imidazole with buffer containing 20 mM HEPES (pH 7.5), 100 mM NaCl, 0.5% (w/v) LMNG, 0.05% (w/v) CHS, 0.00025% (w/v) GDN, 100  $\mu\text{M}$  TCEP and 50  $\mu\text{M}$  (**R**)-**69**. The N-terminal BRIL was removed by addition of His-tagged PresCission protease (GeneScript) with incubation overnight at 4 °C. Protease-cleaved BRIL and uncleaved protein were trapped by equilibrated TALON IMAC resin (Clontech) and the flow-through was collected. The 5-HT<sub>2A</sub>R was further purified by size-exclusion chromatography on the Superdex 200 10/300 gel-filtration column (GE Healthcare) with SEC buffer containing 20 mM HEPES (pH 7.5), 100 mM NaCl, 0.001% (w/v) LMNG, 0.0001% (w/v) CHS, 0.00025% (w/v) GDN, 100  $\mu\text{M}$  TCEP, 1 mM MgCl<sub>2</sub> and 25  $\mu\text{M}$  (**R**)-**69**, and stored until use.

For purification of the G<sub>q</sub> heterotrimeric complex, insect cells (sf9) expressing the miniG<sub>q/i</sub>/ $\beta_1/\gamma_2$  were collected 72 h after infection. Cells were lysed in buffer containing 20 mM HEPES (pH 7.5), 100 mM NaCl, 30 mM imidazole, 5 mM  $\beta$ -mercaptoethanol, 1 mM MgCl<sub>2</sub>, 0.2% (v/v) Triton X-100 and protease inhibitors, and the soluble fraction was isolated by ultracentrifugation at 40,000g at 4 °C for 50 min. The supernatant

was incubated with His60 Ni Superflow resin (Takara) at 4 °C for 2 h. The Ni-NTA resin was washed with 10 column volumes of buffer containing 20 mM HEPES (pH 7.5), 100 mM NaCl, 30 mM imidazole and 5 mM  $\beta$ -mercaptoethanol. The heterotrimeric G protein was eluted using buffer containing 20 mM HEPES (pH 7.5), 100 mM NaCl, 300 mM imidazole and 5 mM  $\beta$ -mercaptoethanol. The PresCission protease (HRV3C protease) was added and the histidine tag was cleaved at 4 °C overnight. The histidine tag-cleaved heterotrimeric G protein was further purified by size-exclusion chromatography on a Superdex 200 10/300 gel filtration column (GE Healthcare) with SEC buffer containing 20 mM HEPES (pH 7.5), 100 mM NaCl, 0.001% (w/v) LMNG, 0.0001% (w/v) CHS, 0.00025% (w/v) GDN and 100  $\mu\text{M}$  TCEP, and collected and concentrated to around 20 mg ml<sup>-1</sup> and stored at -80 °C until use.

The purification process of scFv16 was performed essentially as previously reported<sup>34</sup>. Medium expressing scFv16 from insect cells (sf9) was pH-balanced to pH 8.0 by addition of Tris powder. Chelating agents were quenched by addition of 1 mM nickel and 5 mM CaCl<sub>2</sub> and incubated with stirring for 1 h at 25 °C. The precipitates were removed by centrifugation at 16,263g for 30 min and the supernatant was incubated with His60 Ni Superflow Resin (Takara) for 5 h. The resin was loaded over a Poly-Prep Chromatography column (Bio-Rad) and washed with buffer containing 20 mM HEPES pH 7.5, 100 mM NaCl and 20 mM imidazole. The protein was eluted with buffer containing 20 mM HEPES pH 7.5, 100 mM NaCl and 300 mM imidazole, and treated with PresCission protease to cleave the C-terminal His<sub>8</sub> tag. The cleaved protein was further purified by size-exclusion chromatography using the Superdex 200 10/300 gel-filtration column (GE Healthcare). Monomeric fractions were pooled, concentrated, flash-frozen in liquid nitrogen and stored at -80 °C freezer until use.

Purified 5-HT<sub>2A</sub>R–(**R**)-**69** was mixed with a 1.2 molar excess of miniG<sub>q/i</sub>/ $\beta_1/\gamma_2$  heterotrimer. The coupling reaction was allowed to proceed at 24 °C for 1 h and was followed by addition of 0.2 U ml<sup>-1</sup> (final concentration) of apyrase to catalyse the hydrolysis of free GDP. After 1 h, a 1–1.5 molar excess of scFv16 was added to the 5-HT<sub>2A</sub>R and miniG<sub>q/i</sub>/ $\beta_1/\gamma_2$  mixture and incubated overnight at 4 °C. The 5-HT<sub>2A</sub>R, miniG<sub>q/i</sub>/ $\beta_1/\gamma_2$  and scFv16 mixture was further purified by size-exclusion chromatography on a Superdex 200 10/300 column in SEC buffer containing 20 mM HEPES (pH 7.5), 100 mM NaCl, 0.001% (w/v) LMNG, 0.0001% (w/v) CHS, 0.00025% (w/v) GDN, 25  $\mu\text{M}$  (**R**)-**69**. Peak fractions were concentrated to -17.4 mg ml<sup>-1</sup> for cryo-EM studies.

### Cryo-EM data collection and 3D reconstruction

A volume of 3.5  $\mu\text{l}$  of purified 5-HT<sub>2A</sub>R–miniG<sub>q/i</sub> complex bound to (**R**)-**69** at a concentration of ~17 mg ml<sup>-1</sup> was applied to glow-discharged (50 s at 10 mA) holey carbon grids (Quantifoil R1.2/1.3) under 100% humidity. Excess sample was blotted away for 3 s at 22 °C, and the grids were subsequently plunge-frozen into liquid ethane using a Vitrobot Mark IV (Thermo Fisher Scientific). Cryo-EM imaging was performed on the Titan Krios (Thermo Fisher Scientific) electron microscope operated at 300 kV with a K3 Summit direct electron detector (Gatan) at a magnification of  $\times 57,050$  (0.8521  $\text{\AA}$  px<sup>-1</sup>) in counting mode. A total of 5,140 videos, dose-fractionated over 50 frames, were recorded with a dose rate of 1.2 electrons per  $\text{\AA}^2$  (0.05 s per frame for a total dose of 60 electrons per  $\text{\AA}^2$ ) in super-resolution mode with a defocus range of 0.8–1.8  $\mu\text{m}$  using SerialEM<sup>66</sup>. Cryo-EM data processing was performed using Relion (v.3.1)<sup>67</sup>. Dose-fractionated image stacks were processed for beam-induced motion correction and dose-weighting using MotionCor2<sup>68</sup>. Contrast transfer function parameters for corrected micrographs were determined using CTFIND-4.1 in Relion. Particles were selected using the reference-based picking algorithm in Relion. A total of 4,038,793 particles were extracted from the corrected 5,140 micrographs. Multiple 2D and 3D classification rounds were performed. A subset of 88,393 particles was subjected to CTF refinement and two rounds of Bayesian polishing before final refinement and sharpening was applied. The resolution of the final map at the 0.143 FSC threshold

was estimated to be 3.38 Å by Mtriage in Phenix and 3.45 Å by Relion v.3.1 (Extended Data Table 4).

### Model building and refinement

The active-state structure of 5-HT<sub>2A</sub>R–miniG<sub>q/i</sub> complex bound to NBOH (PDB: 6WHA)<sup>15</sup> was used as an initial model for docking into the EM density map using Chimera<sup>61</sup>. The 5-HT<sub>2A</sub>R/(R)-69 starting model was processed for iterative rounds of manual refinement in Coot<sup>69</sup> and real-space refinement in Phenix<sup>70</sup>. Model statistics were validated using Molprobity<sup>71</sup>. Final refinement statistics are provided in Supplementary Table 1. UCSF Chimera<sup>61</sup> and ChimeraX<sup>72</sup> were used for map/model visualizations and figure preparation. The (R)-69 pose was corroborated using the GemSpot pipeline<sup>35</sup>.

### Mice

Adult male and female C57BL/6J (000664; Jackson Labs) or wild-type and vesicular monoamine transporter 2 (VMAT2) heterozygous (HET) mice were used in the behavioural experiments. Details on the VMAT2 mice have been published previously<sup>73</sup>. No wild animals were used in these experiments and the present investigations did not involve field studies. The mice were housed 3–5 mice per cage according to sex and genotype in a temperature- (21.1–22.2 °C) and humidity- (42–28%) controlled room under a 14 h–10 h (lights on at 06:00) light–dark cycle with food and water provided ad libitum. For the learned helpless experiments, mice that received foot-shock during training were housed individually throughout the study. All experiments were conducted during the light cycle (anhedonia testing was performed during the dark cycle) with an approved protocol from the Duke University Institutional Animal Care and Use Committee and were performed in accordance with relevant regulations and ARRIVE guidelines.

### Drugs

The synthesis of (R)-69 and (R)-70 is described above. The (+)-LSD-(+)-tartrate (LSD) and psilocin (NIDA Drug Supply Program) were used as psychedelical controls, and fluoxetine (FLX; Sigma-Aldrich), MDL 100907 and SB 242084 (Bio-Techne) were used as controls in the tail suspension test with VMAT2 mice. In the learned helplessness study, psilocin (NIDA Drug Supply Program) and ketamine (Henry Schein) were used as controls. In the behavioural sensitization and conditioned place preference studies, cocaine (Sigma-Aldrich) was used as a control and its vehicle was water (Mediatech). The vehicle for all other drugs/compounds was composed of *N,N*-dimethylacetamide (final volume 0.5%; Sigma-Aldrich) that was brought to volume with 5% 2-hydroxypropyl-β-cyclodextrin (Sigma-Aldrich) in water (Mediatech). All drugs were administered (i.p.) at a 5 ml kg<sup>-1</sup> volume.

### Behavioural methods

The sample sizes for these experiments were determined by previous experience. Mice were randomly assigned to different treatment groups, except for learned helplessness, which is described below. All of the experiments were conducted in a blinded manner; the statistical analyses were dummy coded and annotated subsequently so that the outputs were interpretable. The individuals who conducted the experiments were different from the people who statistically analysed the data. Moreover, (R)-69 and (R)-70 were given labels that were different from these names.

**Open field.** This apparatus was described previously<sup>73</sup>. C57BL/6J mice were placed into the open field for 30 min, injected with vehicle, 1 or 3 mg kg<sup>-1</sup> (R)-69 or (R)-70, or 0.3 mg kg<sup>-1</sup> LSD, and returned to the open field for 30 min. For LSD blockade, 1 or 3 mg kg<sup>-1</sup> (R)-69 or 3 mg kg<sup>-1</sup> (R)-70 was administered and the mice were placed into the open field. After 30 min, the mice were removed and injected with LSD and returned to the open field for 30 min. Locomotion was monitored using Fusion Integra software (Omnitech) and expressed as distance travelled. *n* = 8 mice

for 1 mg kg<sup>-1</sup> (R)-69 + 0.3 mg kg<sup>-1</sup> LSD; *n* = 9 mice for 0.3 mg kg<sup>-1</sup> LSD; *n* = 10 mice for vehicle, 1 or 3 mg kg<sup>-1</sup> (R)-69, 1 mg kg<sup>-1</sup> (R)-70, 3 mg kg<sup>-1</sup> (R)-69 + 0.3 mg kg<sup>-1</sup> LSD, or 3 mg kg<sup>-1</sup> (R)-70 + 0.3 mg kg<sup>-1</sup> LSD; and *n* = 11 mice for the 3 mg kg<sup>-1</sup> (R)-70 treatments.

**Head-twitch responses.** These behaviours were filmed during the open-field studies over the 30 min interval immediately after drug administration. Head-twitch responses were scored by individuals blinded to the treatments of the mice. The numbers of mice used in each treatment group are provided in the ‘Open field’ section above.

**Prepulse inhibition.** This test and apparatus were described previously<sup>32</sup>. C57BL/6J mice were administered the vehicle, 1 or 3 mg kg<sup>-1</sup> (R)-69 or (R)-70, or 0.3 mg kg<sup>-1</sup> LSD. *n* = 8 mice for LSD; *n* = 9 mice for 1 mg kg<sup>-1</sup> (R)-69; *n* = 11 mice for 3 mg kg<sup>-1</sup> (R)-70; and *n* = 12 mice for the vehicle, 3 mg kg<sup>-1</sup> (R)-69 or 1 mg kg<sup>-1</sup> (R)-70 treatments.

**Conditioned place preference.** This test and apparatus were described previously<sup>74</sup> and C57BL/6J mice were administered the vehicle, 3 mg kg<sup>-1</sup> (R)-69 or (R)-70, or 20 mg kg<sup>-1</sup> cocaine. *n* = 9 mice were administered the vehicle and 3 mg kg<sup>-1</sup> (R)-69, the vehicle and 3 mg kg<sup>-1</sup> (R)-70, or the vehicle and cocaine pairings.

**Behavioural sensitization.** The apparatus was described previously<sup>75</sup>. C57BL/6J mice were placed into the open field for 1 h to collect baseline activity. They were removed, injected with 3 mg kg<sup>-1</sup> (R)-69 or 20 mg kg<sup>-1</sup> cocaine, and returned to the open field for 2 h. This procedure was repeated over 5 consecutive days. A 7 day hiatus was imposed, and the mice were challenged with the same compound and psychostimulant on day 11. Locomotor activity was monitored using Fusion Integra software (Omnitech) and expressed as distance travelled. *n* = 10 mice were injected with 3 mg kg<sup>-1</sup> (R)-69 or 20 mg kg<sup>-1</sup> cocaine.

**Tail suspension.** The apparatus and procedure were described previously<sup>41</sup>. VMAT2 mice received the vehicle, 20 mg kg<sup>-1</sup> FLX, 0.5 or 1 mg kg<sup>-1</sup> (R)-69 or (R)-70. Then, 30 min later, the VMAT2 mice were tested for tail suspension over 6 min and were tested again 24 h after injection. For wild-type mice: *n* = 9 mice were given 20 mg kg<sup>-1</sup> FLX or 0.5 or 1 mg kg<sup>-1</sup> (R)-69; and *n* = 10 mice received vehicle or 0.5 or 1 mg kg<sup>-1</sup> (R)-70. For VMAT HET mice: *n* = 9 mice were given 20 mg kg<sup>-1</sup> FLX or 0.5 or 1 mg kg<sup>-1</sup> (R)-69; *n* = 10 mice received 0.5 or 1 mg kg<sup>-1</sup> (R)-70, and *n* = 11 mice received vehicle injections. In a separate experiment with VMAT2 mice, the effects of the 5-HT<sub>2A</sub>R (MDL 100907) and the 5-HT<sub>2C</sub>R (SB 242084) antagonists were examined as described above. For wild-type mice: *n* = 8 mice were given 1 mg kg<sup>-1</sup> SB; and *n* = 10 mice were injected with vehicle or 0.5 mg kg<sup>-1</sup> MDL. For HET mice: *n* = 9 mice received 1 mg kg<sup>-1</sup> SB; and *n* = 11 mice were administered vehicle or 0.5 mg kg<sup>-1</sup> MDL. C57BL/6J mice that were used in the learned helplessness study were tested as described above on day 0 at 30 min after injection (day 0) and on days 1, 4, 9, 14 and 18 after injection (Fig. 6a). For the learned helplessness experiment, for the non-foot-shock (NFS) condition, *n* = 9 mice were administered 10 mg kg<sup>-1</sup> ketamine; and *n* = 10 mice were given vehicle, 1 mg kg<sup>-1</sup> (R)-70 or 1 mg kg<sup>-1</sup> psilocin. For the FS condition, *n* = 9 mice were given vehicle; and *n* = 10 mice were given 1 mg kg<sup>-1</sup> (R)-70, 1 mg kg<sup>-1</sup> psilocin or 10 mg kg<sup>-1</sup> ketamine treatments.

**Learned helplessness.** The apparatus was described previously<sup>41</sup>. C57BL/6J mice were assigned to the FS or NFS conditions and were individually or group housed, respectively, for the duration of the experiment (Fig. 6a). Mice were habituated to the apparatus on days –19 and –18. At the end of all sessions, mice were returned immediately to their home cages. On days –17 to –9, NFS mice explored the apparatus for 60 min; FS animals also had access to the apparatus but were administered 360 0.15 mA foot-shocks for 2 s (10 s variable intertrial interval) each day. On day –8 mice in the FS condition were tested in

# Article

shock escape (0.15 mA foot shock) for 10 trials (30–90 s intertrial interval) as described previously<sup>41</sup>. From days –7 to –2, mice in the FS condition resumed learned helplessness training; NFS mice continued to explore. The FS mice were randomly exposed to wet bedding and food restriction throughout training. On day –1, animals in the NFS and FS conditions were given 10 trials of shock escape testing. According to their performance in shock escape and sucrose preference testing (see below), they were assigned to four treatments: vehicle, 1 mg kg<sup>-1</sup> (**R**)-70, 1 mg kg<sup>-1</sup> psilocin or 10 mg kg<sup>-1</sup> ketamine and administered these treatments on day 0. On days 3, 7, 11, 15 and 19 after injection, all of the mice were tested for shock escape for 10 trials. The numbers of successful escapes and latencies to escape were determined by MedAssociates software. The numbers of C57BL/6J mice used in each condition and treatment group are provided in the ‘Tail suspension’ section above.

**Sucrose preference.** The outline of the procedure was described previously<sup>41</sup>. The mice in the learned helplessness study were given water–water (W–W) pairings on days –7 to –5 and, once intake was stable, it was followed with 0.6% sucrose–water (S–W) pairings on days –4 to –2. W–S pairings were resumed on days 0, 1, 3, 8, 16 and 20 after injection (Fig. 6a). The position of the sucrose bottle was alternated over days and the total volume consumed over the 2 h period was recorded. The preference for sucrose was calculated as the volume of sucrose consumed minus the volume of water, divided by the total intake volume, yielding a ratio from –1 to +1. Positive scores indicate a preference for sucrose, negative scores indicate a preference for water, and scores approaching ‘0’ represent no preference for sucrose or water. The numbers of C57BL/6J mice in this experiment are presented in the ‘Tail suspension’ section above.

**Elevated zero maze.** This test and apparatus were described previously<sup>32</sup>. The learned helplessness mice were tested on day 13 after drug administration (Fig. 6a). The numbers of mice in this experiment are presented in the ‘Tail suspension’ section above.

**Foot-shock sensitivity.** This test and apparatus were described previously<sup>76</sup>. The reactivity to foot-shock was tested using intensities of 0, 0.1, 0.2 and 0.3 mA on day 21 after drug administration (Fig. 6a).  $n = 10$  mice per intensity.

## Statistics for behavioural studies

Statistical analyses were performed using IBM SPSS Statistics 27 and 28 programs (IBM). The data are presented as mean  $\pm$  s.e.m. As no sex effects were detected, this variable was collapsed in our statistical analyses. All measurements were taken from discrete raw data and, in certain cases, from repeated observations within the same animal (that is, repeated-measures ANOVA). One- or two-way ANOVA, repeated-measures ANOVA and analysis of covariance (ANCOVA) were used (all tests were two-tailed and normally distributed), followed by Bonferroni correction for pairwise comparisons.  $P < 0.05$  was considered to be significant. The numbers of mice in each group represent the number of replicates for a given experiment. All behavioural results are plotted using GraphPad Prism. All primary statistics are provided in Supplementary Table 4.

## Reporting summary

Further information on research design is available in the Nature Research Reporting Summary linked to this article.

## Data availability

The cryo-EM density map and corresponding coordinates for 5-HT<sub>2A</sub>R in complex with the new docking hit (**R**)-69 have been deposited at the Electron Microscopy Data Bank (EMDB) and the Protein Data Bank (PDB), respectively, under the following accession codes: EMD-24378

and 7RAN. The full THP library of compounds may be freely accessed online (<http://thp.docking.org/>). All active compounds are available from the authors on request. Sequences used to generate the 5-HT<sub>2A</sub>R homology model are available at UniProt (P28223 and 5P41595) or from the PDB (4IB4 (chain A), 4NC3 (chain A), 5TVN (chain A)). Figures with associated raw data include Figs. 2 and 3 (the underlying activities are uploaded in the Source Data); Fig. 4 and Extended Data Figs. 4 and 5 (electron density maps and associated files are deposited at the PDB); Fig. 5 (underlying numbers are uploaded in an Excel file); Extended Data Figs. 2, 3 and 6 (underlying activities are uploaded in the Source Data); Extended Data Table 3 (underlying numbers are supplied in Supplementary Table 5); and Supplementary Fig. 3 (underlying numbers are uploaded in an Excel file). Further underlying data are provided in Extended Data Table 4 (cryo-EM data collection, refinement and validation); Supplementary Data 1 (synthesis procedures for active compounds, chemical purity of active ligands, spectra and 3D crystallography structures); and Figs. 5 and 6. Extended Data Figures 7–10 depict the raw data points with mean  $\pm$  s.e.m. (Prism files; GraphPad Software) and Supplementary Table 4 displays the statistics from behavioural data (IBM SPSS, v.27 and v.28). All raw behavioural data are uploaded in Excel files. Source data are provided with this paper.

## Code availability

DOCK3.7 is freely available for non-commercial research at <http://dock.compbio.ucsf.edu/DOCK3.7/>. A web-based version is freely available to all at <http://blaster.docking.org/>.

- Pei, J. & Grishin, N. V. PROMALS3D: multiple protein sequence alignment enhanced with evolutionary and three-dimensional structural information. *Methods Mol. Biol.* **1079**, 263–271 (2014).
- Liu, W. et al. Serial femtosecond crystallography of G protein-coupled receptors. *Science* **342**, 1521–1524 (2013).
- Webb, B. & Sali, A. Comparative protein structure modeling using MODELLER. *Curr. Protoc. Bioinform.* **47**, 5.6.1–5.6.30 (2014).
- Coleman, R. G., Carchia, M., Sterling, T., Irwin, J. J. & Shoichet, B. K. Ligand pose and orientational sampling in molecular docking. *PLoS ONE* **8**, e75992 (2013).
- Southan, C. et al. The IUPHAR/BPS Guide to PHARMACOLOGY in 2016: towards curated quantitative interactions between 1300 protein targets and 6000 ligands. *Nucleic Acids Res.* **44**, D1054–D1068 (2016).
- Salomon-Ferrer, R., Case, D. A. & Walker, R. C. An overview of the Amber biomolecular simulation package. *WIREs Comput. Mol. Sci.* **3**, 198–210 (2013).
- Mysinger, M. M. & Shoichet, B. K. Rapid context-dependent ligand desolvation in molecular docking. *J. Chem. Inf. Model.* **50**, 1561–1573 (2010).
- Wei, B. Q., Baase, W. A., Weaver, L. H., Matthews, B. W. & Shoichet, B. K. A model binding site for testing scoring functions in molecular docking. *J. Mol. Biol.* **322**, 339–355 (2002).
- Word, J. M., Lovell, S. C., Richardson, J. S. & Richardson, D. C. Asparagine and glutamine: using hydrogen atom contacts in the choice of side-chain amide orientation. *J. Mol. Biol.* **285**, 1735–1747 (1999).
- Gallagher, K. & Sharp, K. Electrostatic contributions to heat capacity changes of DNA–ligand binding. *Biophys. J.* **75**, 769–776 (1998).
- Sharp, K. A. Polyelectrolyte electrostatics: salt dependence, entropic, and enthalpic contributions to free energy in the nonlinear Poisson–Boltzmann model. *Biopolymers* **36**, 227–243 (1995).
- Pettersen, E. F. et al. UCSF Chimera—a visualization system for exploratory research and analysis. *J. Comput. Chem.* **25**, 1605–1612 (2004).
- Olsson, M. H. M., Søndergaard, C. R., Rostkowski, M. & Jensen, J. H. PROPKA3: consistent treatment of internal and surface residues in empirical pKa predictions. *J. Chem. Theory Comput.* **7**, 525–537 (2011).
- Wang, L. et al. Accurate and reliable prediction of relative ligand binding potency in prospective drug discovery by way of a modern free-energy calculation protocol and force field. *J. Am. Chem. Soc.* **137**, 2695–2703 (2015).
- Olsen, R. H. J. et al. TRUPATH, an open-source biosensor platform for interrogating the GPCR transducerome. *Nat. Chem. Biol.* **16**, 841–849 (2020).
- Zhang, Y., Yang, Z., Gao, X. & Wu, G. The role of 5-hydroxytryptamine<sub>1A</sub> and 5-hydroxytryptamine<sub>1B</sub> receptors in modulating spinal nociceptive transmission in normal and carrageenan-injected rats. *Pain* **92**, 201–211 (2001).
- Mastrorade, D. N. Automated electron microscope tomography using robust prediction of specimen movements. *J. Struct. Biol.* **152**, 36–51 (2005).
- Zivanov, J. et al. New tools for automated high-resolution cryo-EM structure determination in RELION-3. *eLife* **7**, e42166 (2018).
- Zheng, S. Q. et al. MotionCor2: anisotropic correction of beam-induced motion for improved cryo-electron microscopy. *Nat. Methods* **14**, 331–332 (2017).
- Emsley, P., Lohkamp, B., Scott, W. G. & Cowtan, K. Features and development of Coot. *Acta Crystallogr. D* **66**, 486–501 (2010).
- Liebschner, D. et al. Macromolecular structure determination using X-rays, neutrons and electrons: recent developments in Phenix. *Acta Crystallogr. D* **75**, 861–877 (2019).

71. Williams, C. J. et al. MolProbity: more and better reference data for improved all-atom structure validation. *Protein Sci.* **27**, 293–315 (2018).
72. Pettersen, E. F. et al. UCSF ChimeraX: structure visualization for researchers, educators, and developers. *Protein Sci.* **30**, 70–82 (2021).
73. Fukui, M. et al. Vmat2 heterozygous mutant mice display a depressive-like phenotype. *J. Neurosci.* **27**, 10520–10529 (2007).
74. Berezniuk, I. et al. ProSAAS-derived peptides are regulated by cocaine and are required for sensitization to the locomotor effects of cocaine. *J. Neurochem.* **143**, 268–281 (2017).
75. Pogorelov, V. M. et al. 5-HT<sub>2C</sub> agonists modulate schizophrenia-like behaviors in mice. *Neuropsychopharmacology* **42**, 2163–2177 (2017).
76. Wetsel, W. C. et al. Disruption of the expression of the proprotein convertase PC7 reduces BDNF production and affects learning and memory in mice. *Proc. Natl Acad. Sci. USA* **110**, 17362–17367 (2013).
77. Yempala, T. et al. Dibenzofuranylethylamines as 5-HT<sub>2A/2C</sub> receptor agonists. *ACS Omega* **5**, 2260–2266 (2020).

**Acknowledgements** We thank the staff at the Schrödinger for donating its Maestro and FEP+ packages and programs and OpenEye Scientific for donating the Omega and OEChem programs; E. Montabana for support with data collection; M. Huffstickler, C. Ritter and C. Means for helping with the behavioural testing; and J. Zhou for breeding, genotyping and maintaining the VMAT2 mice; and the staff at the NIDA Drug Supply Program for providing us with (+)-LSD-(+)-tartrate and psilocin. This work was supported by DARPA HRO01119S0092 (to B.L.R., G.S., W.C.W. and B.K.S.) and by NIH grants R35GM122473 (to J.A.E.), R35GM122481 (to B.K.S.), R37DA045657 (to B.L.R.), R01MH11205 (B.L.R. and B.K.S.) and GM71896 (to J.J.I.). Some of the behavioural experiments were conducted with equipment and software purchased with a North Carolina Biotechnology Center grant. The views, opinions and/or findings contained in this material are those of the authors and should not be interpreted as representing the official views, policies or endorsement of the Department of Defense or the US Government.

**Author contributions** The study was conceived by J.A.E., J.J.I. and B.K.S., and was designed by J.A.E., B.L.R., B.K.S., G.S., J.J.I., A.L.K., D.N.C., K.K. and X.B.-Á. A.L.K. conducted the docking calculations and the chemoinformatics. Y.Y. and L.C.M. conducted MD and FEP+ calculations. J.J.I. designed and implemented the virtual library and conducted the chemoinformatics. D.N.C., D.N.K. and O.S.K. synthesized and purified all of the compounds. J.P.P. performed functional group compatibility screens. K.K. conducted the molecular pharmacology, assisted by T.C., J.M., S.T.S., J.M.K. and J.F.D.; X.-P.H. conducted and supervised off-target activity assays. K.K. produced and purified the 5-HT<sub>2A</sub>R, and X.B.-Á. determined the structure of the agonist complex, assisted by M.J.R., O.P. and A.B.S.; R.M.R., V.M.P. and W.C.W. conducted the behavioural studies and were assisted by A.Q.W. These studies were designed by W.C.W. and B.L.R., some of the behavioural methods were written by A.Q.W. and the remainder were written by W.C.W. with data analysis performed by R.M.R. and graphing performed by W.C.W., V.M.P. and R.M.R.; J.A.E., B.L.R., B.K.S., G.S., J.J.I., A.L.K., D.N.C., K.K. and X.B.-Á. drafted the original manuscript. All of the authors reviewed the manuscript before submission.

**Competing interests** J.A.E., D.N.C., O.S.K., B.L.R., K.K., B.K.S., A.L.K. and J.J.I. have filed a patent (WO2022067165) around the new THP agonists through their universities. B.K.S. is a founder of Epiodyne and, with J.J.I., BlueDolphin. B.K.S., J.J.I. and G.S. are co-founders of Deep Apple. B.L.R. is a scientific founder of Onsero Therapeutics. The other authors declare no competing interests.

#### Additional information

**Supplementary information** The online version contains supplementary material available at <https://doi.org/10.1038/s41586-022-05258-z>.

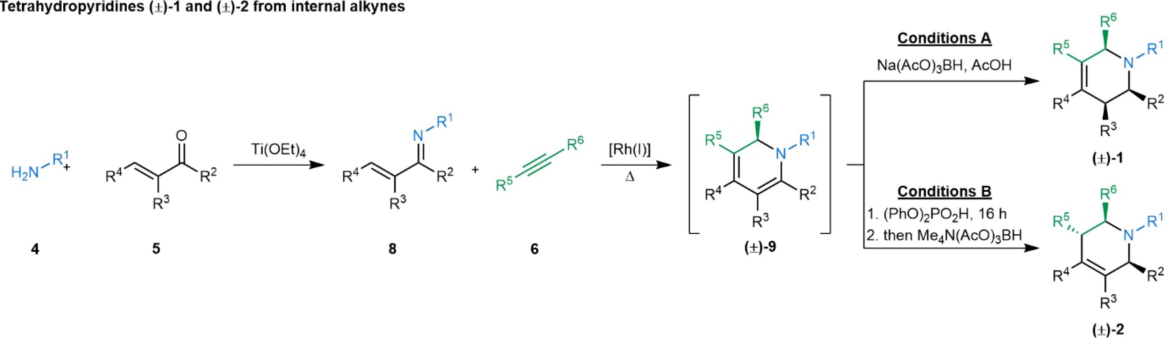
**Correspondence and requests for materials** should be addressed to William C. Wetsel, John J. Irwin, Georgios Skiniotis, Brian K. Shoichet, Bryan L. Roth or Jonathan A. Ellman.

**Peer review information** *Nature* thanks Javier González-Maeso, Christa Mueller and the other, anonymous, reviewer(s) for their contribution to the peer review of this work.

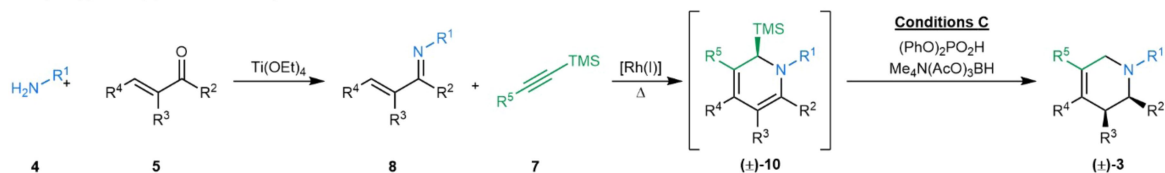
**Reprints and permissions information** is available at <http://www.nature.com/reprints>.



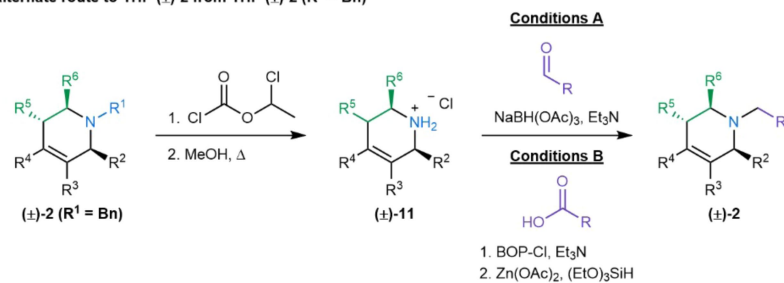
**a** Tetrahydropyridines ( $\pm$ )-1 and ( $\pm$ )-2 from internal alkynes



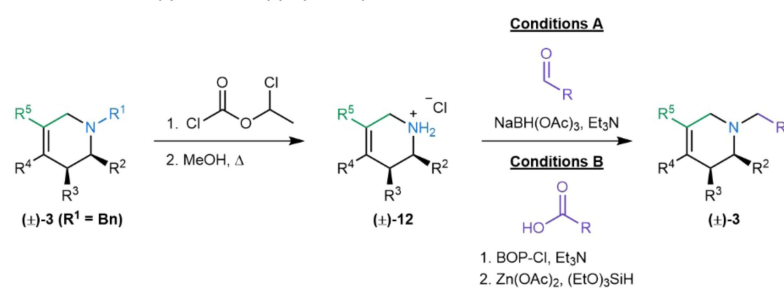
Tetrahydropyridine ( $\pm$ )-3 from TMS alkyne



**b** Alternate route to THP ( $\pm$ )-2 from THP ( $\pm$ )-2 ( $\text{R}^1 = \text{Bn}$ )

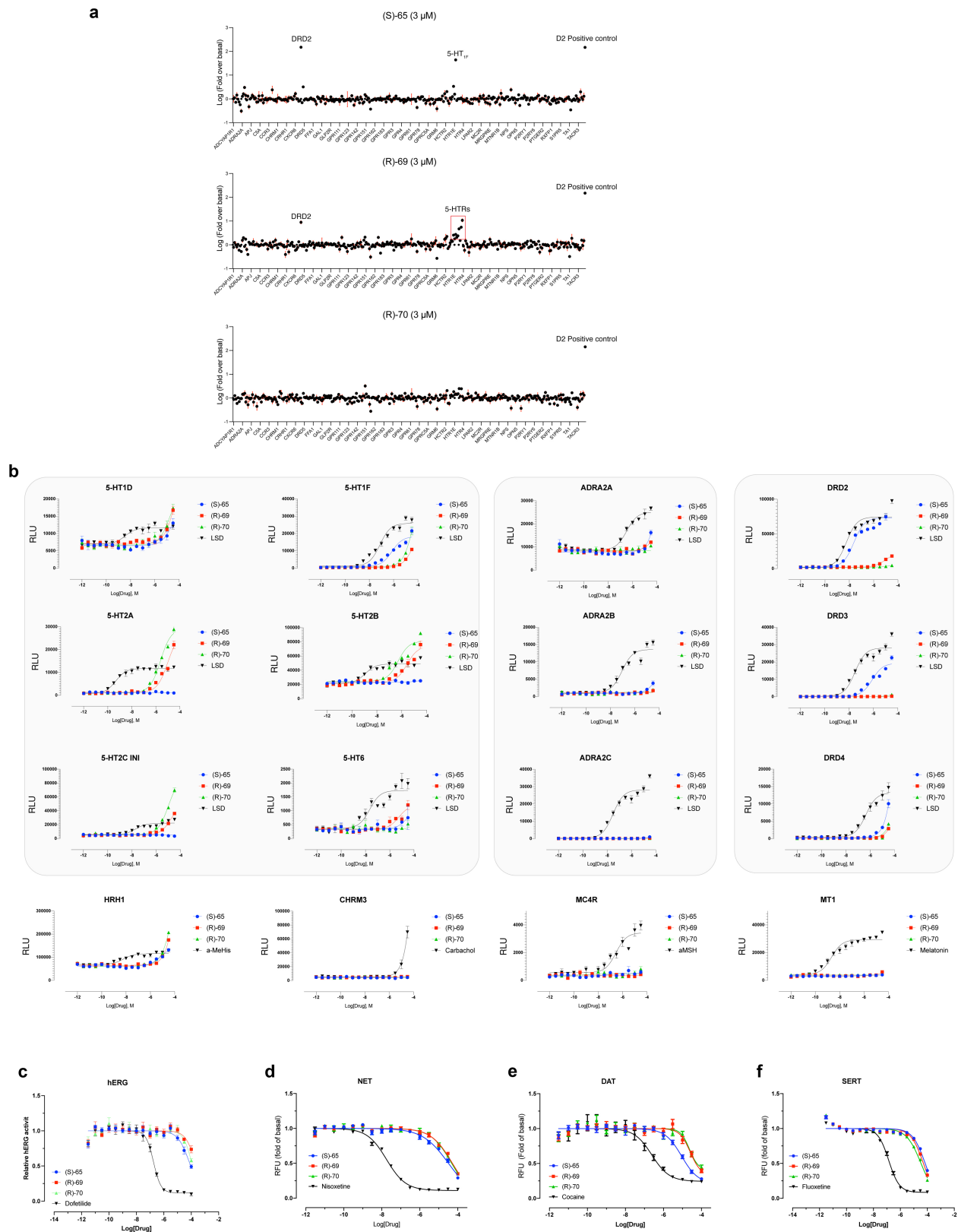


Alternate route to THP ( $\pm$ )-3 from THP ( $\pm$ )-3 ( $\text{R}^1 = \text{Bn}$ )



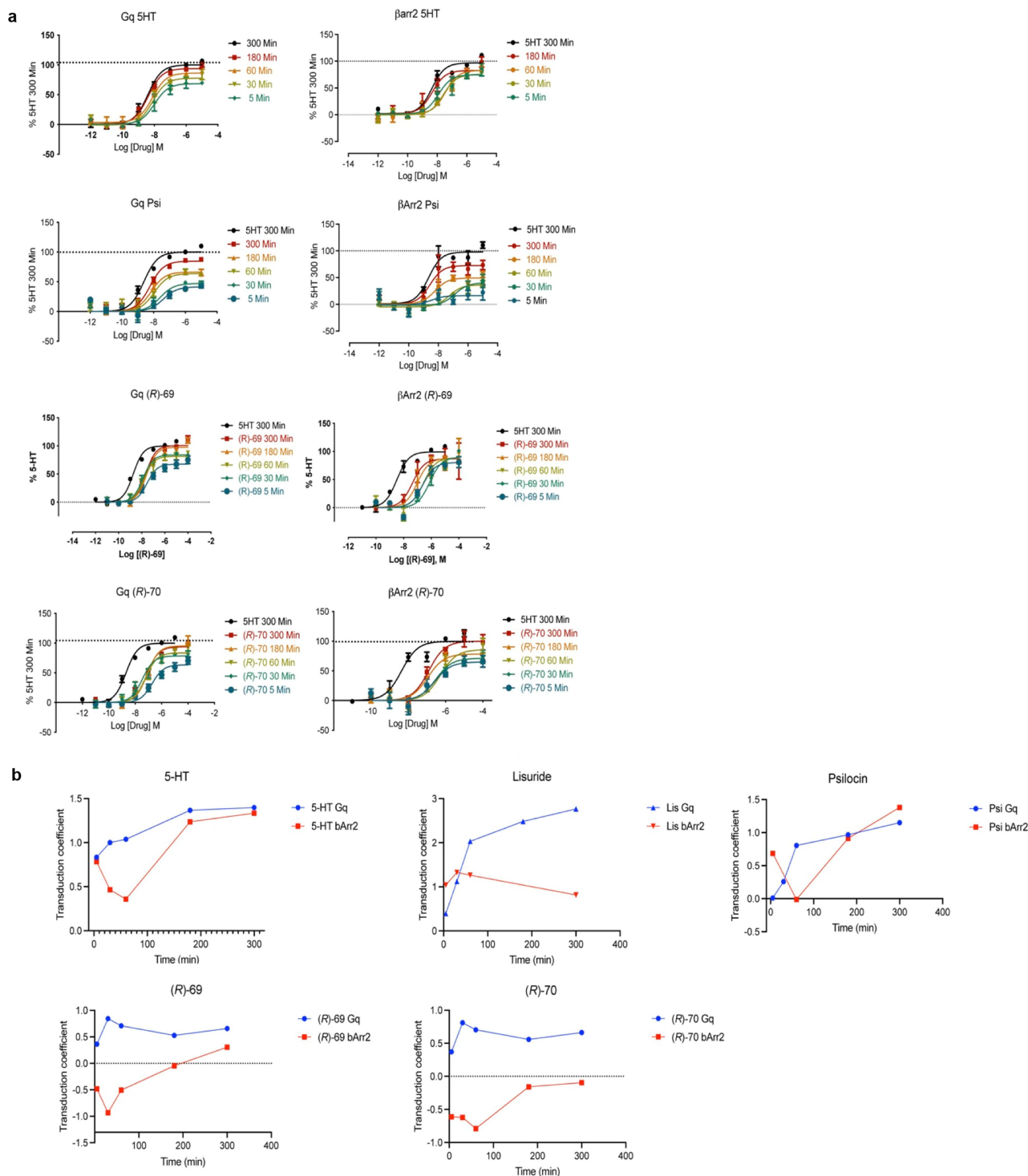
**Extended Data Fig. 1 | (a) Synthetic routes to access densely functionalized, diastereoselective tetrahydropyridines 1 to 3.** Building blocks used for tetrahydropyridines ( $\pm$ )-1 and ( $\pm$ )-2:  $\text{R}^1$ ,  $\text{R}^5$ ,  $\text{R}^6 =$  alkyl, aryl, heteroaryl;  $\text{R}^2 = \text{H}$ , alkyl;  $\text{R}^3$ ,  $\text{R}^4 = \text{H}$ , alkyl, aryl, heteroaryl;  $\text{R}^3$ ,  $\text{R}^4 = \text{H}$ , alkyl, aryl, heteroaryl. Building blocks used for tetrahydropyridines

( $\pm$ )-3:  $\text{R}^1 =$  alkyl;  $\text{R}^5 =$  alkyl, aryl, heteroaryl;  $\text{R}^2 = \text{H}$ , alkyl;  $\text{R}^3$ ,  $\text{R}^4 = \text{H}$ , alkyl, aryl, heteroaryl. See Supplementary Data 1 for detailed reaction conditions and procedures. **(b) Alternate routes for installation of  $\text{R}^1$  substituent.** See Supplementary Data 1 for detailed reaction conditions and procedures.



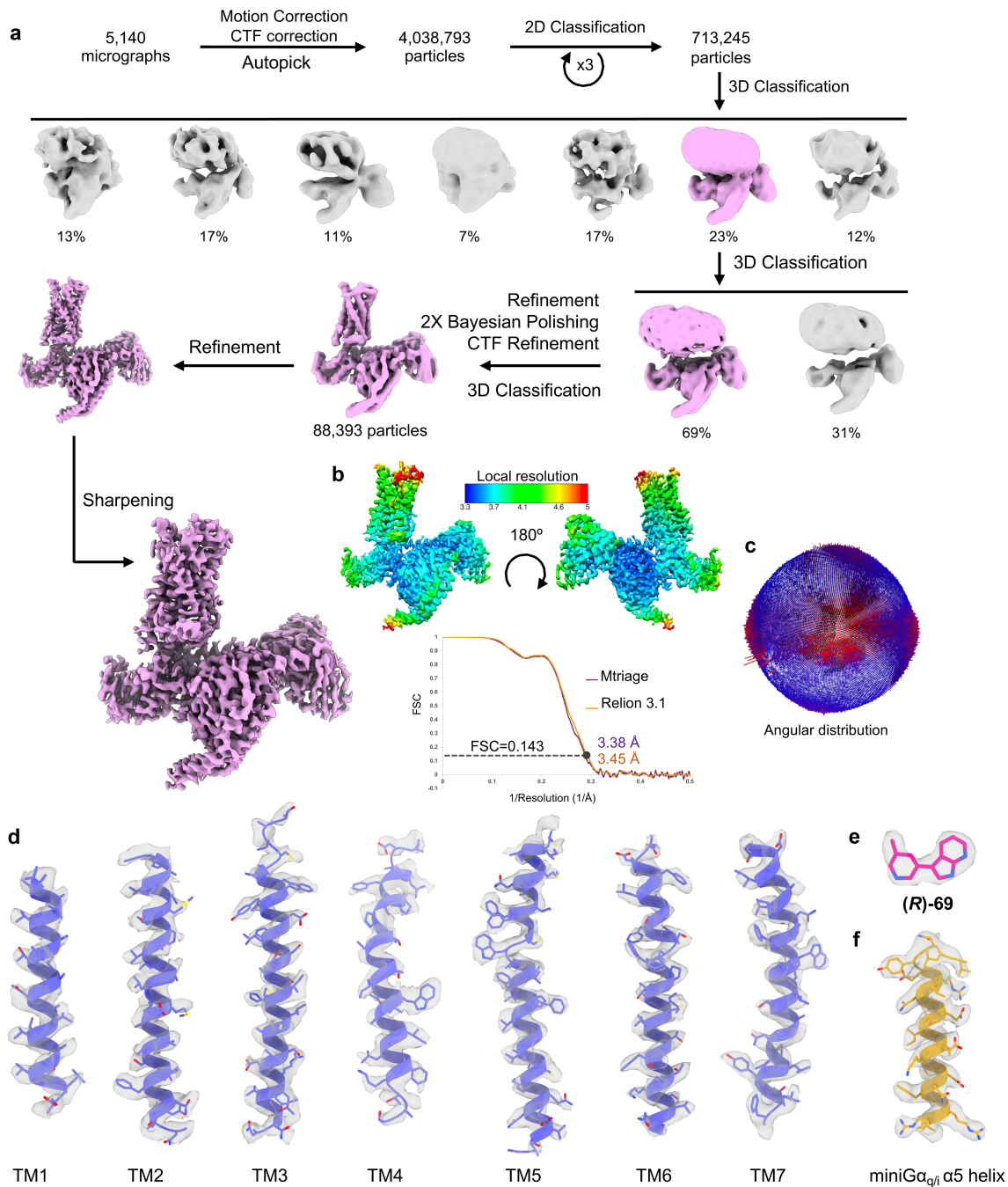
**Extended Data Fig. 2 | Pharmacological profiles of (S)-65, (R)-69, and (R)-70.** (a) Screening of (S)-65, (R)-69, and (R)-70 across the GPCROME (320 receptors) using the PRESTO-Tango platform<sup>10</sup> with agonists present at 3  $\mu$ M concentrations; for visibility, only 1-in-4 receptors are listed on the x-axis. (b) Analysis of the function of (S)-65, (R)-69, and (R)-70 on various receptors shows the diverse

profiles for each receptor. (c)-(f) Binding profiles of (S)-65, (R)-69, and (R)-70 on (c) hERG; human ether-a-go-go-related gene, (d) NET; norepinephrine transporter, (e) DAT; dopamine transporter, and (f) SERT; serotonin transporter. Data in (a), (b), (c), (d), (e) and (f) represent the mean  $\pm$  S.E.M from  $n = 3$  independent experiments.



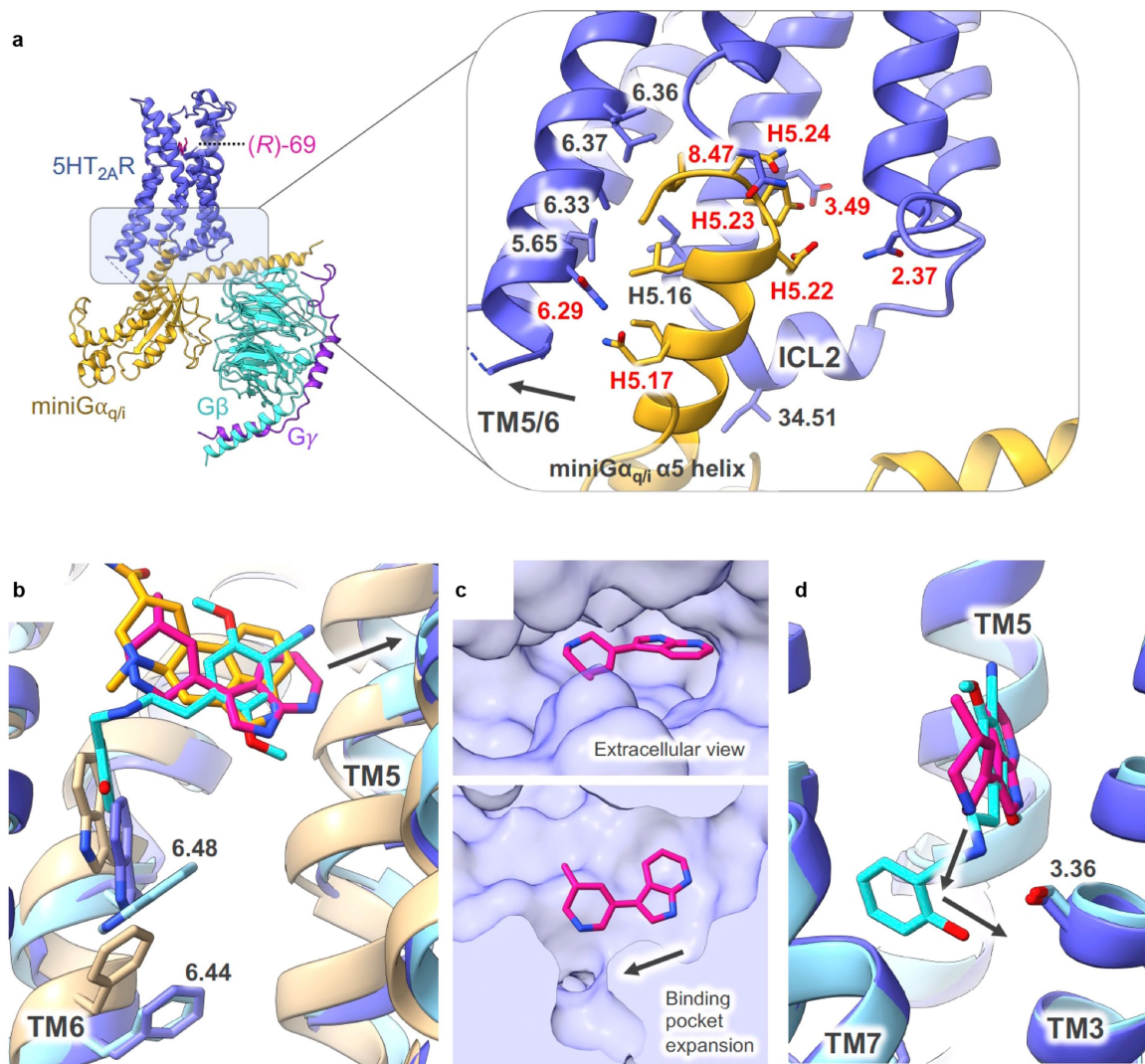
**Extended Data Fig. 3 | Characterization and time course activities of functional bias of (R)-69 and (R)-70 at the human 5-HT<sub>2A</sub>R.** (a) BRET (Gq dissociation and  $\beta$ -Arrestin 2 association) activities of 5-HT (top panel), psilocin (2<sup>nd</sup> panel), (R)-69 (3<sup>rd</sup> panel) and (R)-70 (bottom panel) on the 5-HT<sub>2A</sub>R.

Data represent the mean  $\pm$  SEM from n = 3 independent experiments, each performed in triplicate. (b) Transduction coefficients for Gq and  $\beta$ Arr2 at various time points. Transduction coefficients were measured (see METHODS) for each time point in (a) and then plotted vs time.



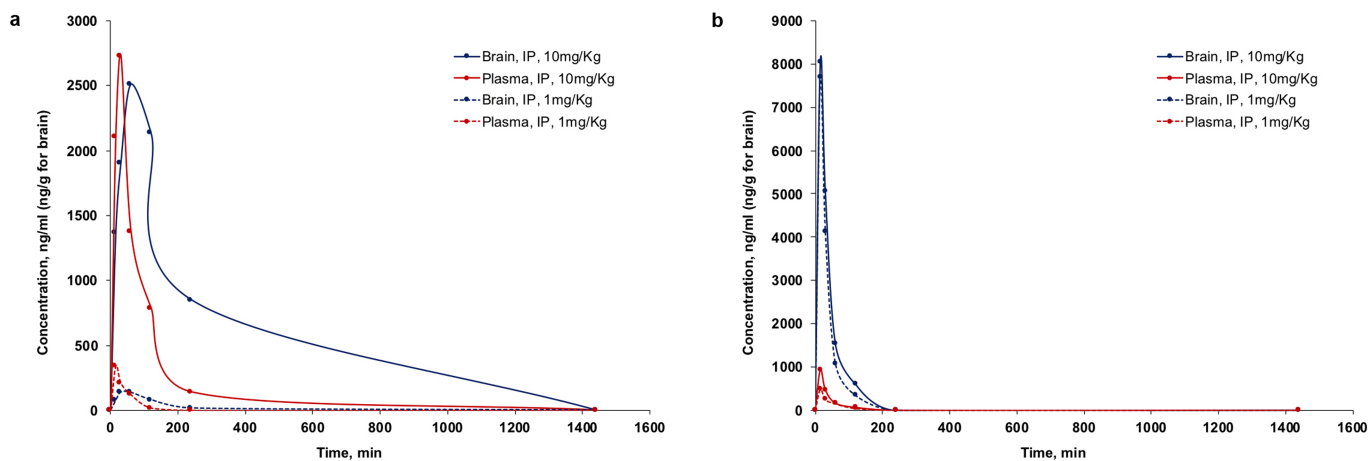
**Extended Data Fig. 4 | Cryo-EM workflow.** (a) Workflow of cryo electron microscopy (cryo-EM) data processing of the 5-HT<sub>2A</sub>R/miniGα<sub>q/i</sub> complex bound to (R)-69. (b) Local resolution estimation heat map and gold standard Fourier shell correlation (FSC) curve. Dashed line represents the overall

nominal resolution at 0.143 FSC of 3.38 Å calculated using Phenix Mtriage and 3.45 Å calculated by Relion 3.1 after post-processing. (c) Angular distribution heat map of particles for cryo-EM reconstruction. (d) Cryo-EM density for TM1-7 of 5-HT<sub>2A</sub>R, E, (R)-69 and F, α5 helix of miniGα<sub>q/i</sub>.



**Extended Data Fig. 5 | Comparison between the cryo-EM structure of (R)-69 bound 5-HT<sub>2A</sub>R/miniGq/i and other 5-HT<sub>2A</sub>R structures.** (a) 5-HT<sub>2A</sub>R-miniGα<sub>q/i</sub> complex interactions. Arrow points to opening of TM5/6 in active (R)-69 bound 5-HT<sub>2A</sub>R state. (R)-69 bound 5-HT<sub>2A</sub>R in blue; miniGα<sub>q/i</sub> in gold. Residues involved in hydrophobic interactions are labelled in grey while residues involved in H-bond interactions are labelled in red. (b) Ligand specific interactions with 5-HT<sub>2A</sub>R. (R)-69 in magenta. LSD bound 5-HT<sub>2A</sub>R structure in

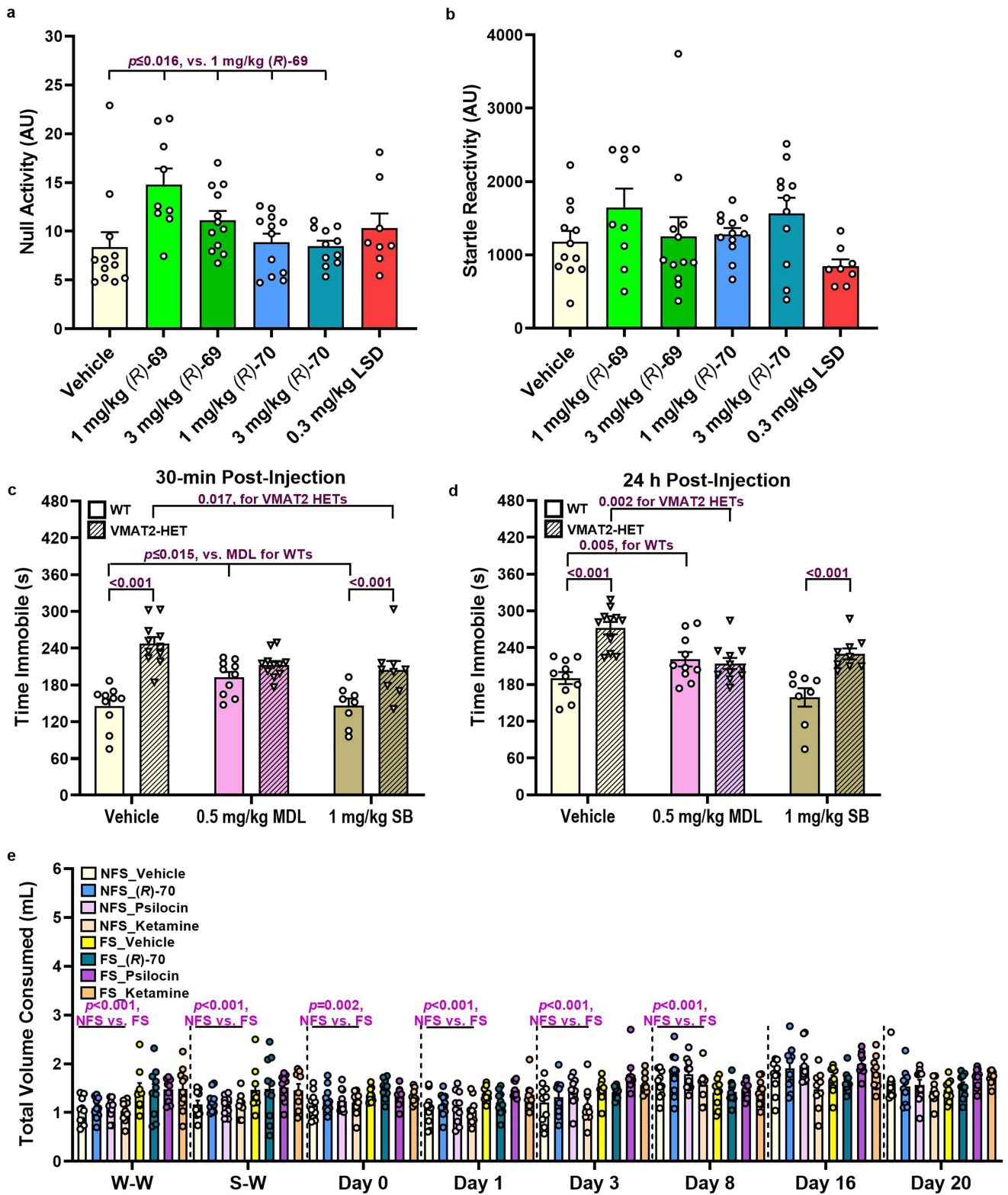
tan; LSD in orange. 25CN-NBOH bound 5-HT<sub>2A</sub>R structure in light cyan; 25CN-NBOH in cyan. Arrow points to extension of (R)-69 and 25CN-NBOH towards TM5. (c) Top: view of the 5-HT<sub>2A</sub>R ligand-binding pocket from the extracellular side; bottom: expansion of binding pocket of 5-HT<sub>2A</sub>R bound to (R)-69 towards the cytosolic side of the receptor. (d) Proposed optimization of (R)-69 to engage in a hydrogen-bond interaction with S159<sup>3,36</sup>. In all panels the Ballesteros-Weinstein numbering is shown in superscript for each residue.



**c**

Sample	Administration	Dose, mg/kg	Pharmacokinetic Parameters					
			T <sub>max</sub> , Min	C <sub>max</sub> , ng/ml (g)	AUC <sub>0→t</sub> (AUC <sub>last</sub> ), ng*min/ml (g)	AUC <sub>0→∞</sub> (AUC <sub>INF_obs</sub> ), ng*min/ml (g)	T <sub>1/2</sub> (HL_Lambda_z), min	K <sub>el</sub> (Lambda_z), min <sup>-1</sup>
<b>(R)-69</b>								
Plasma	IP	1	15.0	344	15900	16600	25.1	0.0276
Brain	IP	1	30.0	139	18600	19800	56.0	0.0124
Plasma	IP	10	30.0	2730	234000	244000	50.8	0.0136
Brain	IP	10	60.0	2510	419000	555000	111	0.00626
<b>(R)-70</b>								
Plasma	IP	1	15.0	487	21300	23700	36.4	0.0191
Brain	IP	1	15.0	7700	267000	279000	23.7	0.0292
Plasma	IP	10	15.0	926	33900	36700	28.8	0.024
Brain	IP	10	15.0	8040	321000	346000	28.2	0.025

**Extended Data Fig. 6 | Pharmacokinetic analysis of (R)-69 and (R)-70.** Concentration-time curves for (R)-69 (a) and (R)-70 (b) in male C57BL/6N mice following IP dosing of either 1 or 10 mg/Kg of the compounds. (c) Selected pharmacokinetic parameters for (R)-69 and (R)-70 in male C57BL/6N mice.

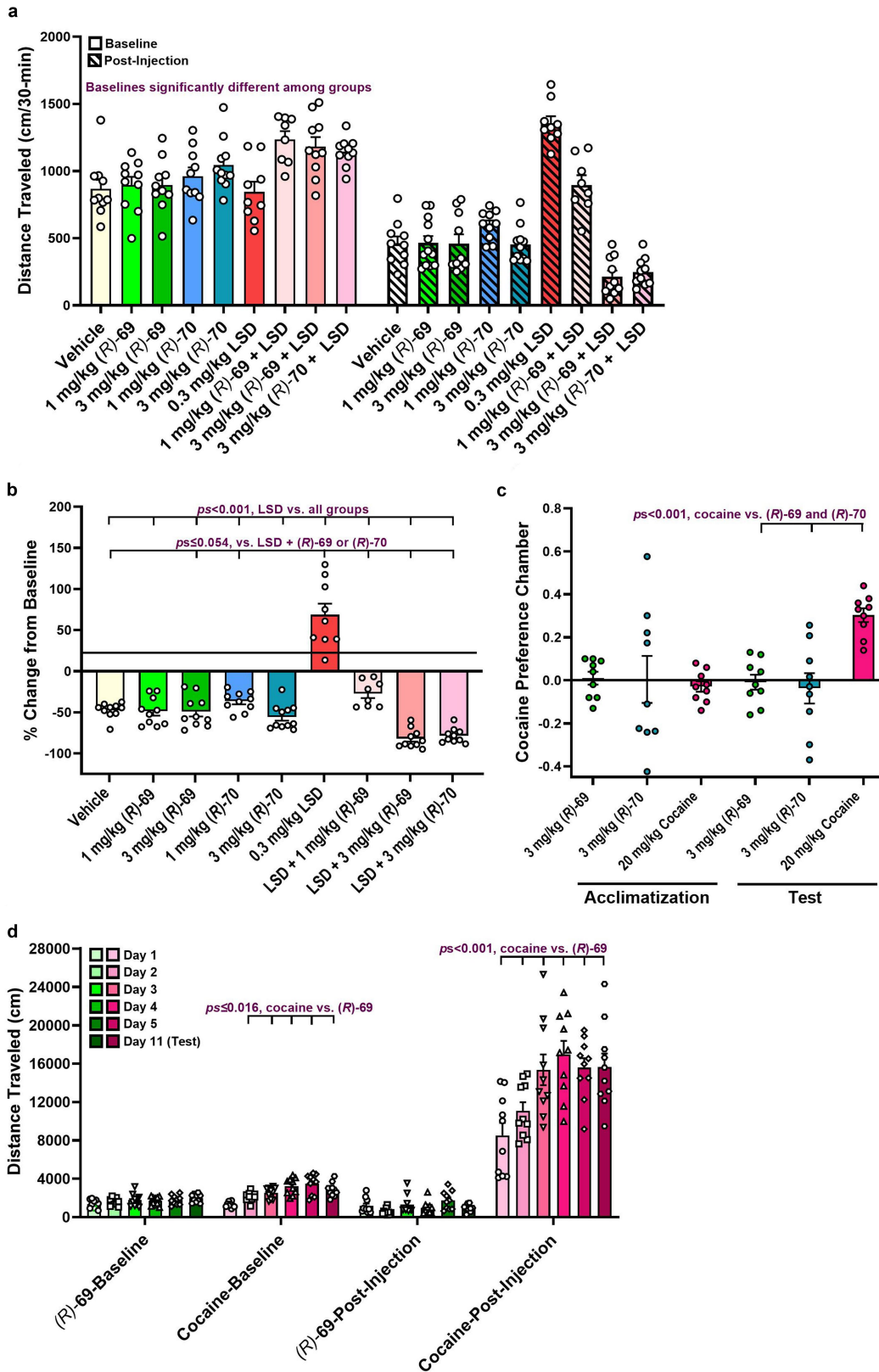


Extended Data Fig. 7 | See next page for caption.

**Extended Data Fig. 7 | Null activity, startle reactivity, antidepressant-like actions of MDL 100907 and SB 242084, and total volume of sucrose and water consumed.** (a) Null activity during PPI for C57BL/6J mice treated (i.p.) with vehicle, 1 or 3 mg/Kg (**R**-69, 1 or 3 mg/Kg (**R**-70, or 0.3 mg/Kg LSD. Null activity increases with 1 mg/Kg (**R**-69 group. (b) Startle reactivity during PPI with C57BL/6J mice undergoing the same treatments. No significant effects are found. (c) Immobility in tail suspension at 30 min and 24 h with WT and VMAT2 HET mice after a single injection (i.p.) of vehicle, 0.5 mg/Kg MDL 100907, or 1 mg/Kg SB 242084. Genotype differences are observed in acute and 24 h tests with vehicle and SB. In WT mice, immobility is increased acutely with MDL compared to vehicle and SB. The difference between the MDL and vehicle groups persists at 24 h. In VMAT2 HETs, immobility times in vehicle controls are

high acutely relative to SB, with a trend ( $p = 0.055$ ) for MDL. At 24 h, immobility times for vehicle-treated mice are higher than for MDL. (e) Total fluid consumed during the sucrose preference test with non-foot-shocked (NFS) and foot-shocked (FS) C57BL/6J mice given (i.p.) vehicle, 1 mg/Kg (**R**-70, 1 mg/Kg psilocin, or 10 mg/Kg ketamine. FS mice drink more than NFS animals during water-water (W-W) and sucrose-water (S-W) pre-test pairings, as well as on post-injection days 0, 1, and 3. Results presented as mean  $\pm$  s.e.m., Ns are found in Methods. Primary statistics are in Supplementary Table 4. In the figure the Bonferroni pair-wise corrected  $p$ -values ( $p_s$ ) across multiple comparisons for 1 mg/kg **R**-69 or MDL showing the value closest to  $p < 0.05$  (respective panels A, C) or within a single comparison ( $p$ ) from the vehicle, MDL, or SB groups (panels C-D), or condition (panel E).



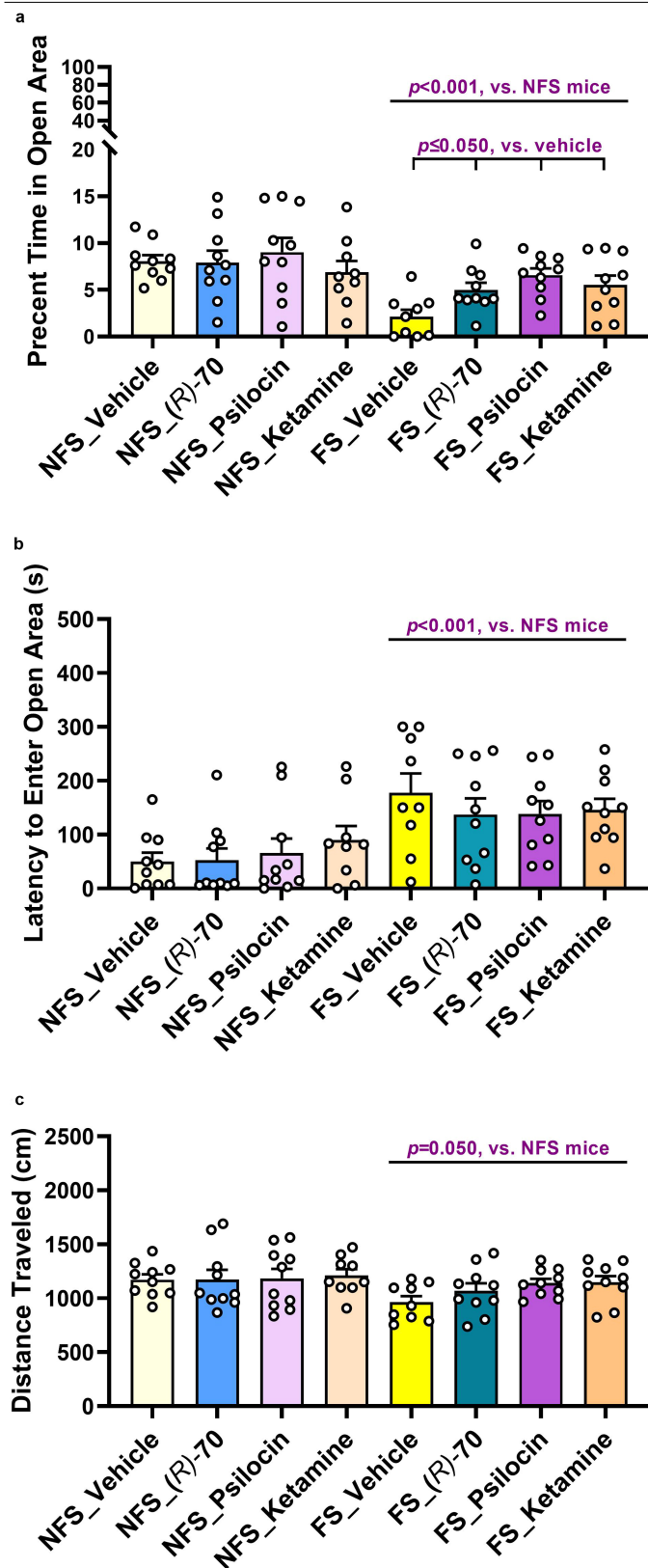


Extended Data Fig. 8 | See next page for caption.

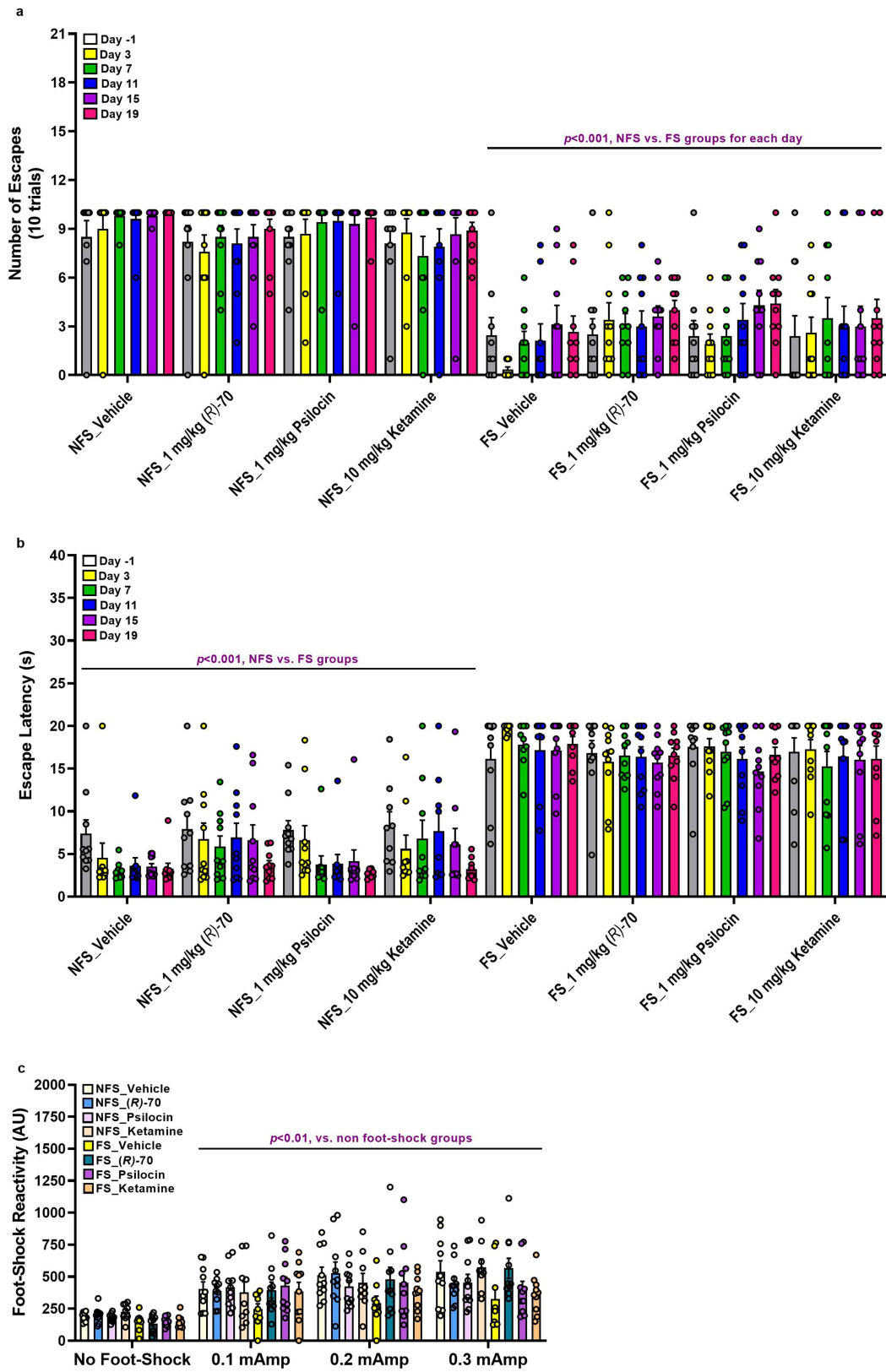
**Extended Data Fig. 8 | Spontaneous locomotion, conditioned place preference (CPP), and behavioural sensitization to (R)-69 and (R)-70.**

(a) Baseline (30 min) and post-injection locomotion (30 min) in C57BL/6J mice after administration (i.p.) of vehicle, 1 or 3 mg/Kg (R)-69, 1 or 3 mg/Kg (R)-70, 0.3 mg/Kg LSD, 1 or 3 mg/Kg (R)-69 + 0.3 mg/Kg LSD, or 3 mg/Kg (R)-70 + 0.3 mg/Kg LSD. Since baseline activities are different among groups, the data are analysed as percent baseline in the next panel. (b) Percent change from baseline from mice in the same experiment. Compared to vehicle, different doses of (R)-69 or (R)-70 have neither stimulatory nor inhibitory effects on locomotion. The compounds blocked LSD-stimulated hyperlocomotion. (c) CPP in C57BL/6J mice to 3 mg/Kg (R)-69, 3 mg/Kg (R)-70, or 20 mg/Kg cocaine (i.p.). No group differences are present at acclimatization, while CPP is evident only in the cocaine group. (d) Behavioural sensitization across 5

consecutive days with a challenge on day 11 using C57BL/6J mice treated (i.p.) with 3 mg/Kg (R)-69 or 20 mg/Kg cocaine. While baseline activities (1 h) are similar between (R)-69- and cocaine-treated mice on day 1, baseline locomotion in the latter group is increased across days 2–5 and at challenge on day 11. Locomotor activities (2 h) are low across all post-injection days for (R)-69 mice, whereby behavioural sensitization to cocaine increases across days 1–3 and remains high through testing. (R)-69-injected mice do not show behavioural sensitization. Results presented as mean  $\pm$  s.e.m. in the figure, Ns are found in Methods. Primary statistics are in Supplementary Table 4. In the figure the Bonferroni pair-wise corrected *p*-values (*ps*) across multiple comparisons to LSD, LSD + (R)-69, or LSD + (R)-70 showing the value closest to  $p < 0.05$  (panel B) or within a single comparison (*p*) from cocaine on specific days (panels C-D).



**Extended Data Fig. 9 | Anxiety-like behaviours in non-foot-shocked (NFS) and foot-shocked (FS) learned helplessness mice.** (a) Percent time in the open areas in the elevated zero maze with C57BL/6J mice treated (i.p.) with the vehicle, 3 mg/Kg (R)-70, 1 mg/Kg psilocin, or 10 mg/Kg ketamine. Animals are tested 13 days post-injection. Mice in the FS condition spend less time in the open areas than NFS animals. Vehicle-treated FS mice spend less time in the open areas than the (R)-70, psilocin, or ketamine FS animals. (b) Latencies to enter the open areas of the maze. Latencies to enter the open areas are prolonged in the FS mice. (c) Distance travelled in the maze. FS mice ambulate within the maze over shorter distances than the NSF animals. Results presented as mean  $\pm$  s.e.m. in the figure, Ns are provided in the Methods section. Primary statistics are found in Supplementary Table 4. In the figure the Bonferroni pairwise corrected  $p$ -values ( $p$ s) across multiple comparisons for vehicle showing the treatment value closest to  $p < 0.05$  (panel A) or within a single comparison ( $p$ ) from condition (panels A-C).



Extended Data Fig. 10 | See next page for caption.

# Article

**Extended Data Fig. 10 | Numbers of escapes, latency to escape, and foot-shock reactivity in non-foot-shocked (NFS) and foot-shocked (FS) learned helplessness mice.** (a) Number of escapes from foot-shock in C57BL/6J mice treated (i.p.) with the vehicle, 1 mg/Kg (**R**)-70, 1 mg/Kg psilocin, or 10 mg/Kg ketamine. All mice assigned to the FS condition have fewer escapes from foot-shock than the NFS animals. (b) Latency to escape from foot-shock in the same experiment. All mice in the FS condition have prolonged escape latencies compared to NFS animals. (c) Reactivity to foot-shock in the same experiment. No significant differences in response to foot-shock are detected among

treatment groups or between mice in the NFS or FS conditions. All mice exposed to foot-shock (i.e., 0.1-0.3 mA) respond at a similar magnitude and this is higher than in the absence of foot-shock (0 mA). Results presented as mean  $\pm$  s.e.m. in the figure, Ns are provided in the Methods section. Primary statistics are found in Supplementary Table 4. In the figure the Bonferroni pairwise corrected  $p$ -values ( $p$ s) across multiple comparisons to 0 mA showing the intensity closest to  $p < 0.05$  (panel C) or within a single comparison ( $p$ ) from condition (panels A-B).

**Extended Data Table 1 | Occurrence of THP, piperidine and pyridine containing molecules in different chemical libraries**

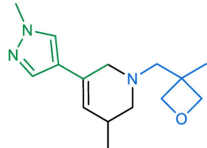
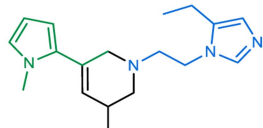
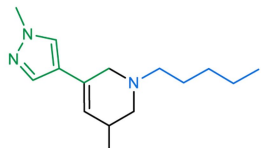
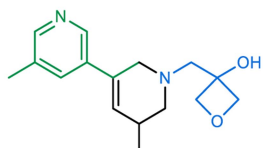
<b>Library</b>	<b>Size</b>	<b>No. THPs (%)</b>	<b>No. piperidines (%)</b>	<b>No. pyridines (%)</b>
World drugs*	2953	20 (0.68%)	274 (9.28%)	287 (9.72%)
Natural products†	307,815	366 (0.12%)	29,193 (9.48%)	26,049 (8.46%)
In Stock lead-like‡	10M	9463 (0.09%)	1.17M (11.7%)	1.28M (12.8%)
Make-on-demand‡	1.35B	4.76M (0.35%)	213M (15.8%)	240M (17.8%)

\*From <https://zinc20.docking.org/substances/subsets/world>.

†From <https://zinc20.docking.org/substances/subsets/biogenic>.

‡Enamine REAL, <http://zinc20.docking.org>.

Extended Data Table 2 | Molecules with activity at the 5-HT<sub>2</sub>R subtypes identified in the initial screen

Cmpd	Structure	5-HT <sub>2A</sub> R		5-HT <sub>2B</sub> R		5-HT <sub>2C</sub> R	
		K <sub>i</sub> (μM) pK <sub>i</sub> ± S.E.M	EC <sub>50</sub> (μM) {pEC <sub>50</sub> ± S.E.M} (E <sub>max</sub> ± S.E.M)	K <sub>i</sub> (μM) pK <sub>i</sub> ± S.E.M	EC <sub>50</sub> (μM) {pEC <sub>50</sub> ± S.E.M} (E <sub>max</sub> ± S.E.M)	K <sub>i</sub> (μM) pK <sub>i</sub> ± S.E.M	EC <sub>50</sub> (μM) {pEC <sub>50</sub> ± S.E.M} (E <sub>max</sub> ± S.E.M)
(±)-26		ND <sup>a</sup>	ND <sup>a</sup>	3.88 {5.41 ± 0.09}	1.94 {5.71 ± 0.12} 48.9 % ± 2.6	ND <sup>a</sup>	ND <sup>a</sup>
(±)-27		6.23 {5.21 ± 0.08}	antagonist	2.67 {5.57 ± 0.12}	2.98 {5.53 ± 0.14} 56.3 % ± 4.1	ND <sup>a</sup>	ND <sup>a</sup>
(±)-28		ND	>10	1.48 {5.83 ± 0.14}	antagonist	ND <sup>a</sup>	ND <sup>a</sup>
(±)-29		ND	ND	0.67 {6.17 ± 0.08}	antagonist	ND <sup>a</sup>	ND <sup>a</sup>

<sup>a</sup>ND no measurable activity up to 10 μM.

**Extended Data Table 3 | Off-target binding profile for compounds (R)-69 and (R)-70 of 45 receptors tested**

Target	pKi ± SEM	
	(R)-69	(R)-70
5-HT <sub>1B</sub> R	5.32 ± 0.08	N.D. <sup>a</sup>
5-HT <sub>1E</sub> R	6.23 ± 0.18	5.90 ± 0.13
5-HT <sub>6</sub> R	6.46 ± 0.02	5.50 ± 0.11
5-HT <sub>7A</sub> R	5.84 ± 0.27	5.49 ± 0.14
α <sub>2A</sub> -adrenergic receptor	5.25 ± 0.12	5.47 ± 0.05
α <sub>2B</sub> - adrenergic receptor	5.42 ± 0.15	5.71 ± 0.08
α <sub>2C</sub> - adrenergic receptor	5.73 ± 0.13	5.68 ± 0.14
Histamine H1 receptor	5.89 ± 0.16	6.19 ± 0.01
Histamine H3 receptor	N.D. <sup>a</sup>	5.71 ± 0.02
M3 muscarinic acetylcholine receptor	<5	N.D. <sup>a</sup>
M4 muscarinic acetylcholine receptor	<5	<5
M5 muscarinic acetylcholine receptor	<5	<5
Mu Opioid receptor	5.66 ± 0.07	N.D. <sup>a</sup>
SERT	6.18 ± 0.12	5.69 ± 0.12
Sigma 1 receptor	N.D. <sup>a</sup>	5.53 ± 0.24
Sigma 2 receptor	5.48 ± 0.01	5.89 ± 0.05

45 targets were evaluated for off-target binding by radio-ligand displacement. Those showing better than 50% displacement at 10 μM or lower compound are shown here. The full list of 45 is given in SI Table 5. <sup>a</sup>N.D. no measurable activity up to 10 μM.



Structure PDB ID	5HT <sub>2A</sub> R-miniG <sub>q/i</sub> -(R)-69 7RAN
<b>Data collection</b>	
Magnification	57,050
Voltage (kV)	300
Dose per frame (e <sup>-</sup> /Å <sup>2</sup> )	1.20
Electron exposure (e <sup>-</sup> /Å <sup>2</sup> )	60.01
Defocus Range (μm)	-0.8 to -1.8
Pixel size (Å)	0.8521
Processing software	Relion 3.1
Symmetry imposed	C1
Number of Micrographs	5140
Initial particle images (no.)	4,038,793
Final particle images (no.)	88,393
Map resolution (Å)	3.38 (Mtriage) / 3.45 (Relion)
FSC threshold	0.143
<b>Refinement Statistics<sup>#</sup></b>	
Model Resolution (Å)	3.5
FSC threshold	0.5
Map sharpening B factor (Å <sup>2</sup> )	82.03
<b>Model composition</b>	
Total number of atoms	8523
Protein	8507
Ligand	16
Number of residues	1120
<b>Model validation</b>	
CC (mask) map vs. model (%)	81
R.m.s. deviations	
Bond lengths (Å)	0.003
Bond angles (°)	0.627
Ramachandran plot	
Favored (%)	97
Outlier (%)	0
Rotamer outliers (%)	0
Clash score	4.9
Molprobity score	1.43

<sup>#</sup>Reported by Phenix comprehensive cryo-EM validation.

## Reporting Summary

Nature Portfolio wishes to improve the reproducibility of the work that we publish. This form provides structure for consistency and transparency in reporting. For further information on Nature Portfolio policies, see our [Editorial Policies](#) and the [Editorial Policy Checklist](#).

### Statistics

For all statistical analyses, confirm that the following items are present in the figure legend, table legend, main text, or Methods section.

- | n/a                                 | Confirmed  |
|-------------------------------------|--|
| <input type="checkbox"/>            | <input checked="" type="checkbox"/> The exact sample size ( $n$ ) for each experimental group/condition, given as a discrete number and unit of measurement  |
| <input type="checkbox"/>            | <input checked="" type="checkbox"/> A statement on whether measurements were taken from distinct samples or whether the same sample was measured repeatedly  |
| <input type="checkbox"/>            | <input checked="" type="checkbox"/> The statistical test(s) used AND whether they are one- or two-sided<br><i>Only common tests should be described solely by name; describe more complex techniques in the Methods section.</i>   |
| <input checked="" type="checkbox"/> | <input type="checkbox"/> A description of all covariates tested  |
| <input type="checkbox"/>            | <input checked="" type="checkbox"/> A description of any assumptions or corrections, such as tests of normality and adjustment for multiple comparisons  |
| <input type="checkbox"/>            | <input checked="" type="checkbox"/> A full description of the statistical parameters including central tendency (e.g. means) or other basic estimates (e.g. regression coefficient) AND variation (e.g. standard deviation) or associated estimates of uncertainty (e.g. confidence intervals) |
| <input type="checkbox"/>            | <input checked="" type="checkbox"/> For null hypothesis testing, the test statistic (e.g. $F$ , $t$ , $r$ ) with confidence intervals, effect sizes, degrees of freedom and $P$ value noted<br><i>Give <math>P</math> values as exact values whenever suitable.</i>                            |
| <input checked="" type="checkbox"/> | <input type="checkbox"/> For Bayesian analysis, information on the choice of priors and Markov chain Monte Carlo settings  |
| <input checked="" type="checkbox"/> | <input type="checkbox"/> For hierarchical and complex designs, identification of the appropriate level for tests and full reporting of outcomes  |
| <input checked="" type="checkbox"/> | <input type="checkbox"/> Estimates of effect sizes (e.g. Cohen's $d$ , Pearson's $r$ ), indicating how they were calculated  |

*Our web collection on [statistics for biologists](#) contains articles on many of the points above.*

### Software and code

Policy information about [availability of computer code](#)

**Data collection** CryoEM data was collected on a Titan Krios (ThermoFisher) using SerialEM 3.8beta and EPU2.6.1.69REL. DOCK3.7.2, Glide SP, MODELER27-9v15, SerialEM V3.8.2 for CryoEM data, MedAssociates for tail suspension data. The anhedonia data were collected by hand and transcribed to Excel and SPSS statistics programs. All data were collected by blinded observers.

**Data analysis** AMBER v18 (2017), Qniff 2.2, Marvin v 15.11.23.0, Corina v.3.6.0026, Omega v.2.5.1.4, Maestro 2020-2, FEP+, MotionCor2 (v1.2.6), CTFFIND4 (v4.1), RELION (v3.1), UCSF Chimera (v1.15), UCSF ChimeraX (v1.1), Pymol (v2.4.2), Coot (v0.9.5), Phenix (v1.19.2-4158), GemSpot - Maestro (v2019-4), MolProbity (v4.5.1), GraphPad Prism 9.0, ChemDraw 20.0, Fusion Integra, IBM SPSS Statistics 27.

For manuscripts utilizing custom algorithms or software that are central to the research but not yet described in published literature, software must be made available to editors and reviewers. We strongly encourage code deposition in a community repository (e.g. GitHub). See the Nature Portfolio [guidelines for submitting code & software](#) for further information.

### Data

Policy information about [availability of data](#)

All manuscripts must include a [data availability statement](#). This statement should provide the following information, where applicable:

- Accession codes, unique identifiers, or web links for publicly available datasets
- A description of any restrictions on data availability
- For clinical datasets or third party data, please ensure that the statement adheres to our [policy](#)

The cryo-EM density map and corresponding coordinates for 5-HT2AR in complex with the new docking hit (R)-69 have been deposited in the Electron Microscopy Data Bank (EMDB) and the Protein Data Bank (PDB), respectively, under the following accession codes: EMDB entry ID EMD-24378 and PDB entry ID 7RAN. The full THP library of compounds may be freely accessed at <http://thp.docking.org/>. All active compounds are available from the authors upon request. Sequences used to

generate the 5-HT<sub>2A</sub>R homology model are available from the Uniprot database (<https://www.uniprot.org>, accession numbers: P28223, 5P41595, or from the PDB (<https://www.rcsb.org>, accession codes: 4IB4 (chain A), 4NC3 (chain A), 5TVN (chain A)). Figures with associated raw data include Figs. 2 and 3, the underlying activities are uploaded in an Excel file; Fig. 4, Extended Data Figs. 4 and 5: electron density maps and associated files are deposited with the PDB; Fig. 5, underlying numbers are uploaded in an Excel file; Extended Data Figs. 2, 3 and 6, underlying activities are uploaded in an Excel file; Extended data table 3, underlying numbers are supplied in supplementary table 5. Supplementary Fig. 3, underlying numbers are uploaded in an Excel file. Further underlying data are provided in Extended Data Table 4 (cryoEM data collection, refinement & validation), Supplementary Data 1 (synthesis procedures for active compounds, chemical purity of active ligands, spectra and 3D crystallographic structures), and Figures 5 and 6. Extended Data Figures 7-10 depict the raw data points with means and SEMs (Prism files; GraphPad Software, San Diego, CA) and the Supplementary Table 4 displays the statistics from behavioral data (IBM SPSS, versions 27 and 28). All raw behavioral data are uploaded in Excel files.

## Field-specific reporting

Please select the one below that is the best fit for your research. If you are not sure, read the appropriate sections before making your selection.

Life sciences  Behavioural & social sciences  Ecological, evolutionary & environmental sciences

For a reference copy of the document with all sections, see [nature.com/documents/nr-reporting-summary-flat.pdf](https://www.nature.com/documents/nr-reporting-summary-flat.pdf)

## Life sciences study design

All studies must disclose on these points even when the disclosure is negative.

Sample size	The sample sizes were chosen according to many years of past experience with these behavioral assays with mice. Statistical analyses were run and because we had statistically-significant results, it was unnecessary to run power analyses to increase the Ns. Sample sizes were not predetermined by statistical methods. For cryoEM data, sample sizes were determined by availability of microscope. CryoEM data was collected until we were able to refine a high-resolution structure that allowed us to obtain a high-resolution reconstruction within the confines of limited microscope time.
Data exclusions	No data were excluded
Replication	Since the data were homogeneous, the replications were performed with the numbers of individual mice that were used in each experiment. For FLIPR, BRET, TANGO and radioligand competitive binding assay, three biologically independent experiments (n=3) were performed. All attempts at replication were successful.
Randomization	C57BL/6J WT and VMAT2 mice were randomly assigned to the different treatment groups such that sex and body weights were equally distributed across all treatment groups. For the functional assay including FLIPR, BRET, TANGO and radioligand binding experiments, randomization is not relevant as no group allocations were performed.
Blinding	The personnel who conducted the experiments were blinded to the genotypes and treatment conditions of the mice. These raw data were uploaded to the Duke University cloud where the original data cannot be modified. The statistical analyses were performed with these data on the cloud. For functional in vitro studies, blinding is not necessary due to the nature of these experiments which does not require subject assessment of the data that may influence the validity of the results.

## Reporting for specific materials, systems and methods

We receive information from authors about some types of materials, experimental systems and methods used in many studies. Here, indicate whether each material, system or method listed is relevant to your study. If you are not sure if a list item applies to your research, read the appropriate section before selecting a response.

### Materials & experimental systems

n/a	Included in the study
<input checked="" type="checkbox"/>	<input type="checkbox"/> Antibodies
<input type="checkbox"/>	<input checked="" type="checkbox"/> Eukaryotic cell lines
<input checked="" type="checkbox"/>	<input type="checkbox"/> Palaeontology and archaeology
<input type="checkbox"/>	<input checked="" type="checkbox"/> Animals and other organisms
<input checked="" type="checkbox"/>	<input type="checkbox"/> Human research participants
<input checked="" type="checkbox"/>	<input type="checkbox"/> Clinical data
<input checked="" type="checkbox"/>	<input type="checkbox"/> Dual use research of concern

### Methods

n/a	Included in the study
<input checked="" type="checkbox"/>	<input type="checkbox"/> ChIP-seq
<input checked="" type="checkbox"/>	<input type="checkbox"/> Flow cytometry
<input checked="" type="checkbox"/>	<input type="checkbox"/> MRI-based neuroimaging

## Eukaryotic cell lines

Policy information about [cell lines](#)

Cell line source(s)

Cell line source(s)	purchased from ATCC (RRID: CVCL_0045). SF9 (Spodoptera frugiperda) insect cells Expression Systems catalog number 94-001S.
Authentication	HEK293T cells were authenticated by the supplier (ATCC) using morphology and growth characteristics, and STR profiling. HEK293 cells were authenticated using morphologies and growth characteristics according to instructions on ThermoFisher website. SF9 insect cells were maintained by the supplier. No additional validation was conducted by authors of this study.
Mycoplasma contamination	HEK293T and HEK293 cell lines tested negative for mycoplasma contamination (Hoechst DNA stain and Direct Culture methods employed). SF9 insect cells were tested negative for mycoplasma by the manufacturer for contamination and no additional testing was conducted by authors of this study.
Commonly misidentified lines (See <a href="#">ICLAC</a> register)	No commonly misidentified cell lines were used in the study.

## Animals and other organisms

Policy information about [studies involving animals](#); [ARRIVE guidelines](#) recommended for reporting animal research

Laboratory animals	Species: <i>Mus musculus</i> ; Genetic Background: C57BL/6J; Genotypes: C57BL/6J, wild-type and <i>Vmat2</i> heterozygotes; sex: males and females; Ages: C57BL/6J -- 4 months old and VMAT2 -- 3-5 months old. The mice were housed 3-5/cage according to sex and genotype in a temperature- and humidity-controlled room on a 14:10 h (lights on at 0600 h) light-dark cycle with food and water provided ad libitum.
Wild animals	No wild animals were used in the study.
Field-collected samples	No field collected samples were used in the study.
Ethics oversight	Animal protocol A077-20-03 approved by the Duke University IACUC

Note that full information on the approval of the study protocol must also be provided in the manuscript.